Chapter 4
Computation of Inter-Nodal Permeabilities for Richards Equation

As shown in Chap. 3, an important problem in the spatial discretization of the unsaturated and two-phase flow equations is related to the averaging of the fluid permeabilities. Various averaging techniques are presented in this chapter, with particular focus on the case of one-dimensional unsaturated flow in a homogeneous medium, for which accurate inter-nodal permeability estimations based on the steady flow analysis are available. It is shown that the relation between capillary and gravity forces at the scale of a single grid cell has key importance for the choice of the averaging scheme. The method proposed by the author is presented in detail, and its extensions to heterogeneous materials and multidimensional problems are discussed. Finally, implications for two-phase flow modelling are considered.

4.1 Overview of Averaging Approaches for One-Dimensional Flow

The averaging methods described below can be used for one-dimensional incompressible unsaturated flow in a homogeneous medium. The water pressure head h_{w} is chosen as the primary variable, in order to facilitate the presentation of the averaging methods based on the analysis of the steady state pressure distribution between nodes. The semi-discrete equation for node j obtained using the finite difference method, Eq. (3.12), can be rewritten as follows:

$$\Delta x^{(\mathrm{ij})} \frac{\mathrm{d}\theta_{\mathrm{w}}^{(j)}}{\mathrm{d}\,t} + v_{\mathrm{w}}^{(\mathrm{jk})} - v_{\mathrm{w}}^{(ij)} = 0 \,, \tag{4.1}$$

where the volumetric fluxes (Darcian velocities) are defined as:

$$v_{\mathrm{w}}^{(ij)} = -K_{\mathrm{sw}}\, k_{\mathrm{rw}}^{(ij)} \left(\frac{h_{\mathrm{w}}^{(j)} - h_{\mathrm{w}}^{(i)}}{\Delta x^{(ij)}} - \zeta \right) , \tag{4.2}$$

A. Szymkiewicz, *Modelling Water Flow in Unsaturated Porous Media*,
GeoPlanet: Earth and Planetary Sciences, DOI: 10.1007/978-3-642-23559-7_4,

$$v_{\mathrm{w}}^{(jk)} = -K_{\mathrm{sw}}\, k_{\mathrm{rw}}^{(jk)} \left(\frac{h_{\mathrm{w}}^{(k)} - h_{\mathrm{w}}^{(j)}}{\Delta x^{(jk)}} - \zeta \right) . \tag{4.3}$$

In the above equations K_{sw} is the saturated conductivity of the water phase and ζ is the cosine of the angle between the x axis and the gravity vector, introduced in Eqs. (3.5) and (3.6). The average relative permeabilities $k_{\mathrm{rw}}^{(ij)}$ and $k_{\mathrm{rw}}^{(jk)}$ can be computed using a number of methods as discussed below.

4.1.1 Simple Averaging Methods

In the simplest approach, if the nodal relative permeabilities are known, the average value can be calculated as one of the well-known algebraic means:

- arithmetic mean:

$$k_{\mathrm{rw}}^{(ij)} = \frac{1}{2} \left(k_{\mathrm{rw}}^{(i)} + k_{\mathrm{rw}}^{(j)} \right) , \tag{4.4}$$

- geometric mean:

$$k_{\mathrm{rw}}^{(ij)} = \sqrt{k_{\mathrm{rw}}^{(i)}\, k_{\mathrm{rw}}^{(j)}} , \tag{4.5}$$

- harmonic mean:

$$k_{\mathrm{rw}}^{(ij)} = \frac{2\, k_{\mathrm{rw}}^{(i)}\, k_{\mathrm{rw}}^{(j)}}{k_{\mathrm{rw}}^{(i)} + k_{\mathrm{rw}}^{(j)}} . \tag{4.6}$$

For the same pair of numbers, the arithmetic averaging yields the largest value of the three methods listed above, while the harmonic averaging—the smallest one. The use of arithmetic mean is well-established in the numerical solution of the unsaturated flow equation, e.g. [11, 23, 25, 35, 43]. It provides relatively accurate results for many typical flow problems, but also has some deficiencies. It tends to overestimate the infiltration rate for capillary-dominated flow, e.g. [19, 21], while for gravity-dominated flow on coarse grids it may lead to unphysical oscillations in the resulting water pressure profile, e.g. [5, 39]. This effect can be considered as equivalent to the oscillations appearing in the solution of linear advection equation using centred in space approximation of fluxes, i.e. it is related to the numerical dispersion.

Geometric averaging yields values of the inter-nodal permeability smaller than the arithmetic averaging. Therefore, it offers some improvement when the arithmetic mean overestimates the flow rate, i.e. during capillary-driven infiltration, e.g. [8, 21, 32]. However, for precisely the same reason, the geometric mean, as compared to the arithmetic mean, leads to larger oscillations and more severe convergence problems in the case of gravity-dominated flow, e.g. [3, 40].

The harmonic mean yields accurate values of the average permeability for steady-state saturated flow in a layered medium in the direction perpendicular to the layers

(see Sect. 2.3.3). While some authors recommended its use also for unsaturated flow in a homogeneous medium [7, 29], in such a case it could be accurate only if the distribution of the relative permeability between nodes were piecewise-constant, i.e. the whole half of the grid cell adjacent to node i had a constant permeability $k_{\mathrm{rw}}^{(i)}$, while the other half, adjacent to node j had a constant permeability $k_{\mathrm{rw}}^{(j)}$. This is not true, since in unsaturated flow the permeability varies continuously between nodes, following the variation of the saturation in a nonlinear manner. Thus, the harmonic mean tends to underestimate the inter-nodal permeability, particularly for downward water infiltration into a dry porous medium. Note that in the limit case of the initial water saturation equal to the residual saturation and the initial relative permeability equal to zero, both geometric and harmonic averaging predict $k_{rw}^{(ij)} = 0$, i.e. no flow at all, which is inconsistent from the physical point of view.

Some schemes are based on the averaging of the argument to the relative permeability function, rather than the relative permeability itself. For example, the inter-nodal permeability can be calculated for the arithmetic average of the nodal saturations:

$$k_{\mathrm{rw}}^{(ij)} = k_{\mathrm{rw}}\left(\frac{S_{\mathrm{w}}^{(i)} + S_{\mathrm{w}}^{(j)}}{2}\right). \tag{4.7}$$

It was shown [28, 30, 46] that this method provides somewhat better results than the averaging of the nodal permeabilities given by Eq. (4.4).

Since in the unsaturated flow the relative permeability is uniquely defined by the water pressure head, the inter-nodal permeability can be calculated using the average of the nodal values of the pressure head:

$$k_{\mathrm{rw}}^{(ij)} = k_{\mathrm{rw}}\left(\frac{h_{\mathrm{w}}^{(i)} + h_{\mathrm{w}}^{(j)}}{2}\right). \tag{4.8}$$

While Eq. (4.8) is rather seldom used, one can note that it is consistent with the finite element approximation of the flux term if linear shape functions and a single-point quadrature rule are used, as discussed in Sect. 3.2.2. Geometric and harmonic averaging of the nodal water pressure heads in the argument of the permeability function in Eq. (4.8) was also tested, but these approaches do not seem to offer any particular advantage [21].

Another averaging method, which was already mentioned in Sect. 3.2.2, is the integrated mean:

$$k_{\mathrm{rw}}^{(ij)} = k_{\mathrm{int}}^{(ij)} = \frac{1}{h_{\mathrm{w}}^{(j)} - h_{\mathrm{w}}^{(i)}} \int_{h_{\mathrm{w}}^{(i)}}^{h_{\mathrm{w}}^{(j)}} k_{\mathrm{rw}}(\hat{h})\,\mathrm{d}\hat{h} = \frac{\Phi_{\mathrm{h}}(h_{\mathrm{w}}^{(j)}) - \Phi_{\mathrm{h}}(h_{\mathrm{w}}^{(i)})}{h_{\mathrm{w}}^{(j)} - h_{\mathrm{w}}^{(j)}}, \tag{4.9}$$

where Φ_h is the flux potential defined with respect to the water pressure head. Following Eq. (2.83) the volumetric water flux can be written in terms of the flux potential as:

$$v_w = -K_{sw}\left(\frac{\partial \Phi_h}{\partial x} - \zeta\, k_{rw}\right), \tag{4.10}$$

or in a discrete form as:

$$v_w^{(ij)} = -K_{sw}\frac{\Phi_h^{(j)} - \Phi_h^{(i)}}{\Delta x^{(ij)}} - \zeta\, K_{sw}\, k_{rw}^{(ij)}. \tag{4.11}$$

For $\zeta = 0$, comparing Eq. (4.11) with the discrete form of the Darcy equation given by Eq. (4.2) results in a formula for $k_{rw}^{(ij)}$ identical with Eq. (4.9). Thus, the integrated mean is an accurate approximation of the inter-nodal conductivity for horizontal unsaturated flow. It was also reported to give accurate results for vertical flow if the node spacing was sufficiently fine, i.e. when the capillary gradient was much larger than the gravity gradient at the scale of a single grid cell [30, 34]. On the other hand, as mentioned in Sect. 3.2.2, the integrated mean results from the exact integration of the flux term in one-dimensional finite element method with linear shape functions used to represent the distribution of p_w or h_w.

Comparative studies available in the literature [6, 21, 30, 34, 36] show that the performance of the simple averaging methods listed above is highly problem-dependent. For example, Haverkamp and Vauclin [21] obtained accurate solutions using geometric averaging, while the simulations presented by Belfort and Lelmann [6] indicated that the geometric mean severely underestimates the flow rate. It is clear that the performance of simple averaging schemes varies according to the following factors: form of the relative permeability function, direction of the flow, initial and boundary conditions and distance between nodes. This observation motivated the development of more accurate averaging methods, in which these factors are at least partially represented. Such methods are described in the following sections.

4.1.2 Direction Dependent Methods

The second group of methods takes into account the direction of the flow. The two most basic approaches are the upstream mean and the downstream mean:

- upstream mean:

$$k_{rw}^{(ij)} = \begin{cases} k_{rw}^{(i)} & \text{if} \quad \dfrac{h_w^{(j)} - h_w^{(i)}}{\Delta x^{(ij)}} - \zeta \le 0 \\ k_{rw}^{(j)} & \text{if} \quad \dfrac{h_w^{(j)} - h_w^{(i)}}{\Delta x^{(ij)}} - \zeta > 0 \end{cases} \tag{4.12}$$

- downstream mean:

$$k_{\mathrm{rw}}^{(ij)} = \begin{cases} k_{\mathrm{rw}}^{(i)} & \text{if} \quad \dfrac{h_{\mathrm{w}}^{(j)} - h_{\mathrm{w}}^{(i)}}{\Delta x^{(ij)}} - \zeta > 0 \\ k_{\mathrm{rw}}^{(j)} & \text{if} \quad \dfrac{h_{\mathrm{w}}^{(j)} - h_{\mathrm{w}}^{(i)}}{\Delta x^{(ij)}} - \zeta \leq 0 \end{cases} \tag{4.13}$$

As mentioned in Chap. 3, in the case of linear advection equation, the upstreaming of the advective flux introduces numerical diffusion, and thus ensures oscillation-free solution at the cost of additional smoothing. Therefore, the upstream mean is the preferred choice for two-phase flow with important contribution of advective (viscous or gravity) terms [16, 22]. It is also recommended for the simulation of gravity-driven unsaturated flow [16]. On the other hand, upstream averaging introduces large errors for capillary-dominated (diffusive) flow, for example in the case of upward flow driven by capillary forces [5, 39, 40].

The downstream mean is practically not used, since it may lead to severe underestimation of the average permeability and, similarly to the geometric and harmonic average, it cannot reproduce infiltration into very dry medium [6]. Moreover, in the case of pure advection equation the use of downstream approximation of the advective fluxes causes instability of solution [14].

The unsaturated water flux consists of two parts. The first one is related to the capillary forces, and has diffusive character, while the other one is related to the gravity forces, and has advective character. In view of this fact, some authors propose to split the flux and use a different permeability averaging scheme for each component:

$$v_{\mathrm{w}}^{(ij)} = -K_{\mathrm{sw}} \left(k_{\mathrm{ca}}^{(ij)} \frac{h_{\mathrm{w}}^{(j)} - h_{\mathrm{w}}^{(i)}}{\Delta x^{(ij)}} - \zeta \, k_{\mathrm{gr}}^{(ij)} \right), \tag{4.14}$$

where $k_{\mathrm{ca}}^{(ij)}$ and $k_{\mathrm{gr}}^{(ij)}$ denote the average relative permeabilities for the capillary and gravity term, respectively. The principal difficulty related to the application of such methods is that if different averaging schemes are used for the capillary and gravity term, the expression:

$$k_{\mathrm{ca}}^{(ij)} \frac{h_{\mathrm{w}}^{(j)} - h_{\mathrm{w}}^{(i)}}{\Delta x^{(ij)}} - \zeta \, k_{\mathrm{gr}}^{(ij)}$$

does not necessarily has the same sign as the water potential gradient:

$$\frac{h_{\mathrm{w}}^{(j)} - h_{\mathrm{w}}^{(i)}}{\Delta x^{(ij)}} - \zeta \ .$$

If this is the case, the flux becomes wrongly oriented leading to physically inadmissible solutions. In particular, depending on the choice of the two permeabilities, this method may predict a non-zero flux for hydrostatic case, when the total potential gradient is equal to zero. Nevertheless, such an approach offers some advantages

over the simple averaging methods, like the arithmetic mean, especially for the case of downward infiltration, when both capillary and gravity gradients are oriented in the same direction.

Taking into account the considerations presented above, a natural choice for $k_{\mathrm{ca}}^{(ij)}$ is the integrated mean $k_{\mathrm{int}}^{(ij)}$, while for the gravity term the upstream mean should be used. Note that in this case the choice of the upstream direction should be based on the gravitational potential, not the total potential, which means that $k_{\mathrm{gr}}^{(ij)}$ is equal to the permeability of the node which is placed higher with regard to the reference level:

$$k_{\mathrm{gr}}^{(ij)} = \begin{cases} k_{\mathrm{rw}}^{(i)} & \text{if} \quad \zeta \geq 0 \,, \\ k_{\mathrm{rw}}^{(j)} & \text{if} \quad \zeta < 0 \,. \end{cases} \tag{4.15}$$

The combination of integrated average for $k_{\mathrm{ca}}^{(ij)}$ and upstream average for $k_{\mathrm{gr}}^{(ij)}$ was used by Zhang and Ewen [47], while Fuhrmann and Langmach [17] applied arithmetic average for $k_{\mathrm{ca}}^{(ij)}$ and the upstream average for $k_{\mathrm{gr}}^{(ij)}$. On the other hand, Zaidel and Russo [46] used the standard arithmetic mean for $k_{\mathrm{gr}}^{(ij)}$, while for $k_{\mathrm{ca}}^{(ij)}$ they developed a simplified formula which approximates $k_{\mathrm{int}}^{(ij)}$ for the relative permeability function of the van Genuchten–Mualem type. Ross [33] also applied the arithmetic average for gravity term in his scheme based on the Kirchhoff transform, but recognized that it should be replaced by a weighted average, with weighting parameters giving more importance to the upper node. In general, if $k_{\mathrm{gr}}^{(ij)}$ is approximated with other schemes than the upstream mean, the monotonicity of the solution is not guaranteed [17].

Equation (4.14) can be transformed to the form of Eq. (4.2):

$$v_{\mathrm{w}}^{(ij)} = -K_{\mathrm{sw}}\, k_{\mathrm{rw}}^{(ij)} \left(\frac{h_{\mathrm{w}}^{(j)} - h_{\mathrm{w}}^{(i)}}{\Delta x^{(ij)}} - \zeta \right) , \tag{4.16}$$

if the inter-nodal permeability for the whole flux term is defined as:

$$k_{\mathrm{rw}}^{(ij)} = \left[k_{\mathrm{ca}}^{(ij)} \frac{h_{\mathrm{w}}^{(j)} - h_{\mathrm{w}}^{(i)}}{\Delta x^{(ij)}} - \zeta\, k_{\mathrm{gr}}^{(ij)} \right] \Bigg/ \left[\frac{h_{\mathrm{w}}^{(j)} - h_{\mathrm{w}}^{(i)}}{\Delta x^{(ij)}} - \zeta \right] . \tag{4.17}$$

4.1.3 Darcian Means

A physically consistent framework for computing inter-nodal permeabilities in the discretized unsaturated flow equation was introduced by Warrick [44]. It is called the Darcian mean approach, because it postulates equivalence between the discrete and differential (continuous) forms of the Darcy equation for steady unsaturated water

flow between nodes $x^{(i)}$ and $x^{(j)}$. Assuming (without the loss of generality) that the saturated conductivity K_{sw} is equal to unity, one can write the following relation:

$$v_{\mathrm{st}}^{(ij)} = -k_{\mathrm{rw}}^{(ij)} \left(\frac{\Delta h_{\mathrm{w}}^{(ij)}}{\Delta x^{(ij)}} - \zeta \right) = -k_{\mathrm{rw}}(h_{\mathrm{w}}) \left(\frac{\mathrm{d}h_{\mathrm{w}}}{\mathrm{d}x} - \zeta \right) , \tag{4.18}$$

where $v_{\mathrm{st}}^{(ij)}$ is the uniform steady flux between nodes and $\Delta h_{\mathrm{w}}^{(ij)} = h_{\mathrm{w}}^{(j)} - h_{\mathrm{w}}^{(i)}$. The differential form of the Darcy equation can be integrated as follows:

$$\int_{x^{(i)}}^{x^{(j)}} \mathrm{d}x = -\int_{h_{\mathrm{w}}^{(i)}}^{h_{\mathrm{w}}^{(j)}} \frac{k_{\mathrm{rw}}(h_{\mathrm{w}})\, \mathrm{d}h_{\mathrm{w}}}{v_{\mathrm{st}}^{(ij)} - \zeta k_{\mathrm{rw}}(h_{\mathrm{w}})} . \tag{4.19}$$

For horizontal flow with $\zeta = 0$ one obtains:

$$\Delta x^{(ij)} = -\frac{1}{v_{\mathrm{st}}^{(ij)}} \int_{h_{\mathrm{w}}^{(i)}}^{h_{\mathrm{w}}^{(j)}} k_{\mathrm{rw}}(h_{\mathrm{w}}) \mathrm{d}h_{\mathrm{w}} . \tag{4.20}$$

Comparing this result with the discrete form of the Darcy equation appearing in Eq. (4.18) gives:

$$k_{\mathrm{rw}}^{(ij)} = \frac{1}{\Delta h_{w}^{(ij)}} \int_{h_{w}^{(i)}}^{h_{w}^{(j)}} k_{\mathrm{rw}}(\hat{h}) \mathrm{d}\hat{h} = k_{\mathrm{int}}^{(ij)} . \tag{4.21}$$

Thus, the integrated mean corresponds to the Darcian mean for horizontal flow.

For $\zeta \neq 0$ the Darcian mean depends on $\Delta x^{(ij)}$ and is different from any of the simple averages listed in the previous section. Analytical solution can be obtained if the relative permeability is an exponential function of h_{w} as defined by Eq. (2.44):

$$k_{\mathrm{rw}}(h_{\mathrm{w}}) = \exp\left(h_{\mathrm{w}}/h_{\mathrm{g}}\right) , \tag{4.22}$$

where $h_{\mathrm{g}} > 0$ is a scaling parameter expressed in terms of the water pressure head. For such a constitutive relationship, the integration of Eq. (4.19) yields [2, 12]:

$$v_{\mathrm{st}}^{(ij)} = \frac{\zeta' \left(k_{\mathrm{rw}}^{(j)} - \exp(\zeta')\, k_{\mathrm{rw}}^{(i)} \right)}{1 - \exp(\zeta')} , \tag{4.23}$$

where:

$$\zeta' = \Delta x^{(ij)}\, \zeta / h_{\mathrm{g}} . \tag{4.24}$$

Making use of the following relationship:

$$\Delta h_{\mathrm{w}} = h_{\mathrm{w}}^{(j)} - h_{\mathrm{w}}^{(i)} = h_{\mathrm{g}}\, \mathscr{L}_k \ , \tag{4.25}$$

where $\mathscr{L}_k = \ln(k_{\mathrm{rw}}^{(j)}/k_{\mathrm{rw}}^{(i)})$, one can define the inter-nodal permeability as:

$$k_{\mathrm{rw}}^{(ij)} = \frac{-v_{\mathrm{st}}^{(ij)}\, \Delta x^{(ij)}/h_{\mathrm{g}}}{\Delta h_{\mathrm{w}}^{(ij)} - \zeta\, \Delta x^{(ij)}} = \frac{\zeta' \left(\exp(\zeta')\, k_{\mathrm{rw}}^{(i)} - k_{\mathrm{rw}}^{(j)}\right)}{(1 - \exp(\zeta'))\ (\mathscr{L}_k - \zeta')} \ . \tag{4.26}$$

The above formula was developed by Baker [2] for the case of $\zeta = 1$, while an equivalent result was obtained by Desbarats [12] for a more general case of arbitrary ζ. Moreover, Baker [2] and Baker et al. [5] showed that the Darcian average varies in the range between the integrated mean ($k_{\mathrm{int}}^{(ij)}$) and the permeability at the upper node ($k_{\mathrm{rw}}^{(i)}$, assuming that the gravity force acts in the direction of x axis). Baker et al. [5] proposed to compute the inter-nodal permeability as a weighted arithmetic average of those two values:

$$k_{\mathrm{rw}}^{(ij)} = \omega_{\mathrm{v}}\, k_{\mathrm{rw}}^{(i)} + (1 - \omega_{\mathrm{v}})\, k_{\mathrm{int}}^{(ij)} \ , \tag{4.27}$$

where ω_{v} is a weighting parameter ranging from 0 to 1. In this work the original formula for ω_{v} [3, 5] is extended for the case of arbitrary ζ:

$$\omega_{\mathrm{v}} = \frac{\left(k_{\mathrm{rw}}^{(i)}\, \exp(\zeta') - k_{\mathrm{rw}}^{(j)}\right) \mathscr{L}_k\, \zeta' - \left(1 - \exp(\zeta')\right)\, \Delta k\, \left(\mathscr{L}_k - \zeta'\right)}{(1 - \exp(\zeta'))\ (\mathscr{L}_k - \zeta') \left(k_{\mathrm{rw}}^{(i)}\, \mathscr{L}_k - \Delta k\right)} \tag{4.28}$$

where $\Delta k = k_{\mathrm{rw}}^{(j)} - k_{\mathrm{rw}}^{(i)}$, and

$$\zeta' = \frac{\Delta x^{(ij)}\, \zeta}{\sqrt{k_{\mathrm{rw}}^{(i)}\, k_{\mathrm{rw}}^{(j)}}} \left.\frac{\partial k_{\mathrm{rw}}}{\partial h_{\mathrm{w}}}\right|_{k_{\mathrm{rw}} = \sqrt{k_{\mathrm{rw}}^{(i)}\, k_{\mathrm{rw}}^{(j)}}} \ . \tag{4.29}$$

It means that the modified gravity coefficient ζ' depends on the derivative of the relative permeability function computed for the geometric mean of the nodal permeabilities. The above formula is exact for the exponential relative permeability function, for which Eqs. (4.27)–(4.28) reduce to Eq. (4.26). As shown by Baker et al. [5] and Baker [3], it is a relatively accurate approximation of the true Darcian mean also for other types of the relative permeability functions. An advantage of such approach is that the inter-nodal permeability always remains in the physically consistent range between $k_{\mathrm{int}}^{(ij)}$, which is the limit value for capillary dominated flow and $k_{\mathrm{rw}}^{(i)}$ which is the limit value for gravity-dominated flow. On the other hand, the relative permeability function must be inverted to obtain $h_{\mathrm{w}}\left(\sqrt{k_{\mathrm{rw}}^{(i)}\, k_{\mathrm{rw}}^{(j)}}\right)$,

which may be impossible to carry out analytically for more complicated functions (e.g. van Genuchten–Mualem model).

In principle, the Darcian means can be computed for an arbitrary relative permeability function by integrating numerically Eq. (4.18) or by solving (also numerically) the steady-state flow equation:

$$-\frac{\partial}{\partial x}k_{\mathrm{rw}}(h_{\mathrm{w}})\left(\frac{\partial h_{\mathrm{w}}}{\partial x}-\zeta\right)=0 \tag{4.30}$$

in the domain $\langle x^{(i)}, x^{(j)}\rangle$ with the boundary conditions $h_{\mathrm{w}} = h_{\mathrm{w}}^{(i)}$ for $x = x^{(i)}$ and $h_{\mathrm{w}} = h_{\mathrm{w}}^{(j)}$ for $x = x^{(j)}$. The resulting value of the steady-state flux can be subsequently used to calculate the inter-nodal permeability. Unfortunately, the numerical solution of steady-state Richards equation is a non-trivial problem in itself, and the amount of work necessary to compute the permeabilities for each pair of nodes at each time step of a transient simulation is prohibitive. Warrick [44] suggested to express the inter-nodal permeability as a weighted arithmetic average of the permeability values at the upper and lower node:

$$k_{\mathrm{rw}}^{(ij)} = \omega_{\mathrm{w}}\, k_{\mathrm{rw}}^{(i)} + (1-\omega_{\mathrm{w}})\, k_{\mathrm{rw}}^{(j)} \tag{4.31}$$

where ω_{w} is a weighting parameter ranging from 0 to 1. For a known grid spacing and relative permeability function it is possible to perform multiple solutions of the steady problem at the preprocessing stage in order to obtain the values of the parameter ω_{w} as a function of the two nodal permeability values. During transient flow simulation, ω_{w} can be interpolated from the table for the considered pair of permeabilities $k_{\mathrm{rw}}^{(i)}$ and $k_{\mathrm{rw}}^{(j)}$. However, if the relative permeability function or the grid spacing change, a new interpolation table must be generated, which requires additional numerical effort.

The method based on Eq. (4.31) was further developed by Gasto et al. [19]. They showed that for Brooks–Corey–Burdine and van Genuchten–Mualem permeability functions, the weighting parameter ω_{w} can be expressed as a function of four variables: $k_{\mathrm{rw}}^{(i)}$, $k_{\mathrm{rw}}^{(j)}$, $\Delta x'$ and n'. For Brooks–Corey model $\Delta x' = \Delta x^{(ij)}/h_{\mathrm{e}}$, where h_{e} is the air entry pressure head, and $n' = 1 + n_{\mathrm{b}}$, while for van Genuchten–Mualem model $\Delta x' = \Delta x^{(ij)}/h_{\mathrm{g}}$, where h_{g} is the pressure scaling parameter expressed in terms of the pressure head, and $n' = n_{\mathrm{g}}$. Gasto et al. [19] fitted a closed form analytical function, which allows to compute ω_{w} directly if the four variables are known. The calculation is performed according to the following formula:

$$\omega_{\mathrm{w}} = \left[1 + \frac{a'\left(k_{\mathrm{rw}}^{(i)}\right)^{b'}\Big/\left(k_{\mathrm{rw}}^{(j)}\right)^{c'}}{1+\beta' n'\left(k_{\mathrm{rw}}^{(i)}\right)^{b'}\Big/\left(k_{\mathrm{rw}}^{(j)}\right)^{c'}}\right]^{-1}, \tag{4.32}$$

with the parameters a', b' and c' defined as follows:

Table 4.1 Fitting parameters used in the formula of [19] for Brooks–Corey (BC) and van Genuchten–Mualem (VG) relative permeability functions

	a'_{10}	a'_{11}	a'_2	b'_{01}	b'_{02}	b'_1	c'_0	β'
BC	0.208	0.634	0.191	0.690	2.294	0.049	0.020	0.008
VG	0.465	0.052	0.112	0.551	1.939	0.057	0.009	0.011

$$a' = \frac{1 - \left(a'_{10} + a'_{11}\,\log n'\right)\,\Delta x'}{1 + a'_2\,(n')^2\,\Delta x'}\,, \tag{4.33}$$

$$b' = \frac{b'_{01}\,n'}{b'_{02}\,n' - 1} - b'_1\,\Delta x'\,, \tag{4.34}$$

$$c' = \frac{b'_{01}\,n'}{b'_{02}\,n' - 1} + c'_0\,\left(n' - 1\right)\,\Delta x'\,. \tag{4.35}$$

Thus, the approximating formula contains altogether eight fitting parameters. Two sets of parameters were provided—one for Brooks–Corey–Burdine and the other one for van Genuchten–Mualem functions. Their values are listed in Table 4.1. This approach is relatively simple to implement, but has some limitations. First, the fitted analytical formula is valid only for $1.05 \le n' \le 5$ and the values of the normalized node spacing $\Delta x' < 1$, which is satisfied when:

$$\Delta x^{(ij)} \le h_\mathrm{e} \quad \text{or} \quad \Delta x^{(ij)} \le h_\mathrm{g}\,. \tag{4.36}$$

The above condition limits the applicability of this approach for coarse textured soils, where the pressure scaling parameter is of the order of a few centimetres. Moreover, adaptation of the method to other types of hydraulic functions would require a new parameter fitting procedure.

4.2 Improved Approximation Scheme

In this section, the averaging method proposed by the author, which also belongs to the Darcian averaging framework, is presented in more detail. The presentation closely follows the original paper [39]. The method is based on the analysis of the approximate shape of steady-state water pressure head profiles. The form of the pressure profile depends on the type of flow and three major cases can be distinguished, as shown in Fig. 4.1. In the following discussion it is assumed (without the loss of generality) that x axis is inclined downward, so that the values of ζ range from 0 to 1. The three basic flow regimes are as follows:

- *Infiltration in dry soil*:

$$-\infty < \Delta h_\mathrm{w}^{(ij)} / \Delta x^{(ij)} < 0\,.$$

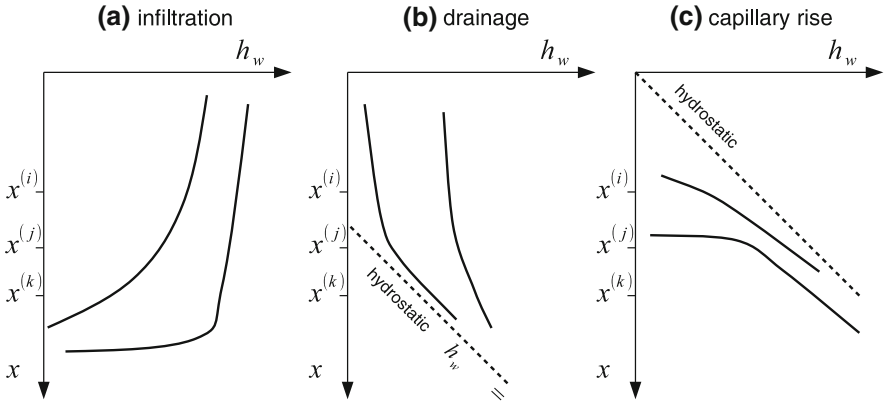

Fig. 4.1 Steady-state profiles of the water potential head for different types of flow (after [45])

In this case, both capillary and gravity forces act in the direction of x axis. In the upper part of the profile the water saturation and relative permeability are larger. Consequently, the gradient in the water pressure is smaller than in the lower part of the domain, in order to ensure uniform flux in both parts. For

$$\Delta h_{\mathrm{w}}^{(ij)} / \Delta x^{(ij)} \to 0$$

the pressure profile tends to a vertical line.

- *Drainage or infiltration close to the water table*:

$$0 < \Delta h_{\mathrm{w}}^{(ij)} / \Delta x^{(ij)} < \zeta \ .$$

In this case, the saturation in the lower part of the domain is larger than in the upper part, but the flow direction is downward, because the capillary potential gradient is smaller than the gravity potential gradient. The pressure profile varies from uniform ($\Delta h_{\mathrm{w}}^{(ij)} / \Delta x^{(ij)} \to 0$) to hydrostatic ($\Delta h_{\mathrm{w}}^{(ij)} / \Delta x^{(ij)} \to \zeta$).

- *Capillary rise or evaporation*:

$$\zeta < \Delta h_{w}^{(ij)} / \Delta x^{(ij)} < \infty \ .$$

The gradients of the capillary and gravity potentials act in the opposite directions. Since the capillary gradient in larger, the flow is in upward direction.

Note that for each flow regime the profiles are monotonous. The differences in profile shapes suggest that for each case a separate averaging formula should be considered. Moreover, three special limit cases can be distinguished:

- *Horizontal flow*: $\zeta = 0$. As shown above, in this case the Darcian mean corresponds to the integrated mean.
- *Uniform pressure distribution*:

$$\Delta h_{\mathrm{w}}^{(ij)} / \Delta x^{(ij)} = 0 \, .$$

  In this case, the average permeability is trivially $k_{\mathrm{rw}}^{(ij)} = k_{\mathrm{rw}}^{(i)} = k_{\mathrm{rw}}^{(j)}$.
- *Hydrostatic pressure distribution*:

$$\Delta h_{\mathrm{w}}^{(ij)} / \Delta x^{(ij)} - \zeta = 0 \, .$$

  In this case, the Darcian averaging principle cannot be used, because both flux and gradient are equal to zero. However, the limit value of the inter-nodal permeability for

$$(\Delta \, h_{\mathrm{w}}^{(ij)} / \Delta x^{(ij)} - \zeta) \to 0$$

  is given by the upstream value $k_{\mathrm{rw}}^{(i)}$ [5].

4.2.1 Infiltration

For infiltration in a dry soil inaccurate approximations of the inter-nodal permeability may lead to two types of errors. For capillary-dominated flow, the correct limit value is given by the integrated mean. Many other averaging methods (in particular the arithmetic or upstream average) overestimate the inter-nodal permeability and consequently predict too large infiltration rates. On the other hand, for gravity-dominated flow all simple averaging methods except the upstream average underestimate $k_{\mathrm{rw}}^{(ij)}$, which leads to oscillatory profile of the water pressure head. The deficiencies of the commonly used averaging methods were shown by Baker [4] on the example of a simple numerical grid consisting of three nodes. Here a similar analysis is performed in order to derive an improved formula for the inter-nodal permeability. It is based on the observation that for steady state unsaturated flow in a homogeneous porous medium the pressure profile resulting form the solution of the Richards equation is monotonous. On coarser numerical grid, the monotonicity can be violated by inaccurate approximation of the inter-nodal permeability, leading to unphysical oscillations (wiggles).

Consider a numerical approximation of steady flow equation on a grid consisting of three nodes, as shown in Fig. 4.2. The flux continuity condition at node j can be written as:

$$-k_{\mathrm{rw}}^{(ij)} \left(\frac{h_{\mathrm{w}}^{(j)} - h_{\mathrm{w}}^{(i)}}{\Delta x^{(ij)}} - \zeta \right) = -k_{\mathrm{rw}}^{(jk)} \left(\frac{h_{\mathrm{w}}^{(k)} - h_{\mathrm{w}}^{(j)}}{\Delta x^{(jk)}} - \zeta \right) . \tag{4.37}$$

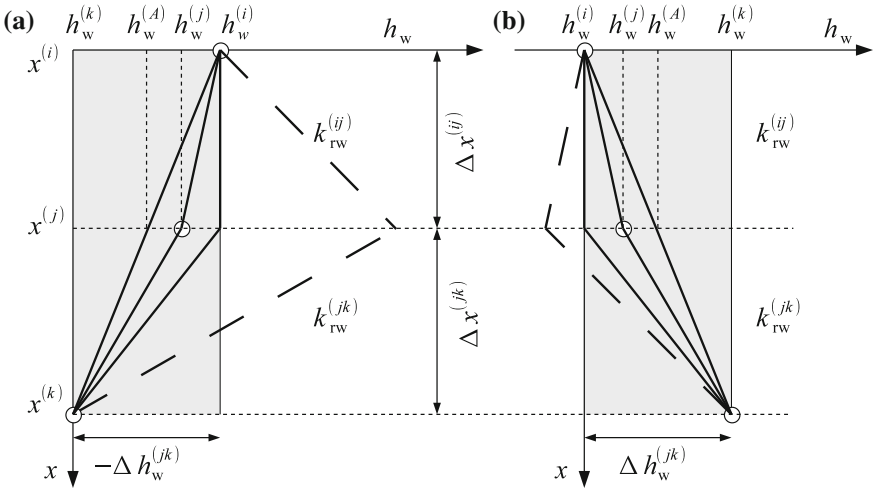

Fig. 4.2 Approximate water pressure head profiles for infiltration (**a**) and drainage (**b**). Modified with permission from [39]

Physically admissible profiles for steady flow are represented by solid lines in Fig. 4.2. The values of the water potential head at the central node $h_w^{(j)}$ should be in the range between $h_w^{(A)}$ and $h_w^{(i)}$, where $h_w^{(A)}$ corresponds to a linear profile and is defined as:

$$h_w^{(A)} = \frac{\Delta x^{(jk)}\, h_w^{(i)} + \Delta x^{(ij)}\, h_w^{(k)}}{\Delta x^{(ij)} + \Delta x^{(jk)}} \,. \tag{4.38}$$

Assuming $h_w^{(j)} = h_w^{(A)}$, the continuity condition given by Eq. (4.37) can be satisfied only if the relative permeability is constant, $k_{rw}^{(ij)} = k_{rw}^{(ik)}$, which is the case for saturated flow. In unsaturated conditions, $k_{rw}^{(ij)} > k_{rw}^{(jk)}$, because the upper part of the medium is more saturated with water. Consequently, if $h_w^{(j)} = h_w^{(A)}$ then $v_w^{(ij)} > v_w^{(jk)}$ and the flux continuity condition is not satisfied. In order to equilibrate the fluxes, the value at the central node j must be larger than $h_w^{(A)}$.

In the second limit case, when $h_w^{(j)} = h_w^{(i)}$ the relative permeabilities at nodes i and j are equal, $k_{rw}^{(i)} = k_{rw}^{(j)}$, and the capillary pressure gradient is zero. The flux in the upper part of the column can be written as:

$$v_w^{(ij)} = \zeta\, k_{rw}^{(i)} = \zeta\, k_{rw}^{(j)} \,, \tag{4.39}$$

while the flux between the nodes j and k can be written as:

$$v_w^{(jk)} = -k_{rw}^{(jk)} \left(\frac{\Delta h_w^{(jk)}}{\Delta x^{(jk)}} - \zeta \right) . \tag{4.40}$$

If the following condition holds:

$$v_{\mathrm{w}}^{(ij)} \leq v_{\mathrm{w}}^{(jk)} \,, \tag{4.41}$$

then one can be sure that there exists a value of the pressure head $h_{\mathrm{w}}^{(j)}$ between $h_{\mathrm{w}}^{(A)}$ and $h_{\mathrm{w}}^{(i)}$, for which $v_{\mathrm{w}}^{(ij)} = v_{\mathrm{w}}^{(jk)}$. Inequality (4.41) together with Eqs. (4.39) and (4.40) imply the following condition for the inter-nodal permeability $k_{\mathrm{rw}}^{(jk)}$:

$$k_{\mathrm{rw}}^{(jk)} \geq \frac{\zeta \; k_{\mathrm{rw}}^{(j)}}{\zeta - \Delta h_{\mathrm{w}}^{(jk)} / \Delta x^{(jk)}} \,. \tag{4.42}$$

If the applied averaging method underestimates the permeability $k_{\mathrm{rw}}^{(jk)}$, the fluxes are not in equilibrium even for $h_{\mathrm{w}}^{(j)} = h_{\mathrm{w}}^{(i)}$ and the profile becomes non-monotonous, as shown by the dashed line in Fig. 4.2. The maximum amplitude of the wiggle cannot exceed $\Delta x^{(ij)}$, since for $h_{\mathrm{w}}^{(j)} = h_{\mathrm{w}}^{(i)} + \Delta x^{(ij)}$ one obtains a hydrostatic potential distribution between $x^{(i)}$ and $x^{(j)}$, and thus $v_{\mathrm{w}}^{(ij)} = 0 < v_{\mathrm{w}}^{(jk)}$ for any value of $k_{\mathrm{rw}}^{(jk)}$. Equation (4.42) represents a sufficient condition, although not a necessary one, for a non-oscillating solution. In some situations physically admissible profiles can be obtained for smaller values of $k_{\mathrm{rw}}^{(jk)}$, but the use of the presented approximation guarantees a monotonous solution for all cases. Note that as $\Delta h_{\mathrm{w}}^{(jk)}$ tends to zero, the limit permeability value from Eq. (4.42) tends to the upstream mean $k_{\mathrm{rw}}^{(jk)} = k_{\mathrm{rw}}^{(j)}$, while, on the other hand, the upstream mean always satisfies the condition given by Eq. (4.42). This is consistent with the findings of other authors who recommended the use of upstream mean to ensure monotonous solution of the Richards equation [15, 16].

In the case of capillary dominated flow, $(\Delta h_{\mathrm{w}}^{(jk)} / \Delta x^{(jk)}) \to -\infty$ and consequently the lower limit for $k_{\mathrm{rw}}^{(jk)}$ given by Eq. (4.42) tends to zero. On the other hand, it is known that for capillary dominated flow the appropriate averaging method is the integrated mean $k_{\mathrm{int}}^{(jk)}$. Therefore, one can use the integrated mean as long as it satisfies the condition Eq. (4.42) and then switch to the limit value given by Eq. (4.42). To summarize, the inter-nodal relative permeability between any two adjacent nodes j (upper) and k (lower) can be computed according to the following formula:

$$k_{\mathrm{rw}}^{(jk)} = \max\left(k_{\mathrm{int}}^{(jk)}, \frac{\zeta \; k_{\mathrm{rw}}^{(j)}}{\zeta - \Delta h_{\mathrm{w}}^{(jk)} / \Delta x^{(jk)}} \right) . \tag{4.43}$$

This method requires only slightly more computational effort than the integrated mean approach.

4.2.2 Drainage

A similar reasoning can be applied to derive the limit value of the average permeability for drainage as $(\Delta h_{\mathrm{w}}^{(jk)}/\Delta x^{(jk)}) \to 0$. This case is shown in Fig. 4.2b. Physically admissible profiles are obtained for values of $h_{\mathrm{w}}^{(j)}$ in the range between $h_{\mathrm{w}}^{(i)}$ and $h_{\mathrm{w}}^{(A)}$, the latter one being interpolated linearly according to Eq. (4.38). In unsaturated conditions, $k_{\mathrm{rw}}^{(ij)}$ is smaller than $k_{\mathrm{rw}}^{(jk)}$ and consequently the total water potential gradient in the lower part of the domain should be smaller than in the upper part. In the limit case when $h_{\mathrm{w}}^{(j)} = h_{\mathrm{w}}^{(i)}$ the average permeability $k_{\mathrm{rw}}^{(jk)}$ should satisfy the following condition:

$$\zeta k_{\mathrm{rw}}^{(j)} \geq -k_{\mathrm{rw}}^{(jk)} \left(\frac{h_{\mathrm{w}}^{(k)} - h_{\mathrm{w}}^{(j)}}{\Delta x^{(jk)}} - \zeta \right) . \tag{4.44}$$

Inequality (4.44) can be transformed to the following form:

$$k_{\mathrm{rw}}^{(jk)} \leq \frac{\zeta k_{\mathrm{rw}}^{(j)}}{\zeta - \Delta h_{\mathrm{w}}^{(jk)}/\Delta x^{(jk)}} . \tag{4.45}$$

If $k_{\mathrm{rw}}^{(jk)}$ is overestimated and does not satisfy Eq. (4.45), the water fluxes $v_{\mathrm{w}}^{(ij)}$ and $v_{\mathrm{w}}^{(jk)}$ equilibrate for a value of the water pressure head $h_{\mathrm{w}}^{(j)} < h_{\mathrm{w}}^{(i)}$, producing a wiggle in the pressure head profile, shown with the dashed line in Fig. 4.2b. The value of $h_{\mathrm{w}}^{(j)}$ will not exceed $h_{\mathrm{w}}^{(k)} - \Delta x^{(jk)}$, for which a zero gradient of the total water potential in the lower part of the domain is obtained. As in the previous case, Eq. (4.45) gives a sufficient, although not a necessary condition to obtain a monotonous solution.

The limit value of $k_{\mathrm{rw}}^{(jk)}$ defined by Eq. (4.45) tends to infinity as the value of the capillary gradient $\Delta h_{\mathrm{w}}^{(jk)}/\Delta x^{(jk)}$ approaches ζ. In such a case, another formula is necessary. It can be obtained from an analysis of the approximate potential head profile within a singe grid cell between nodes j and k, as shown in Fig. 4.3. Let us assume that $\Delta x^{(jk)}$ is larger than $\Delta h_{\mathrm{w}}^{(jk)}$ only by a small value $\Delta x^{(jD)}$, i.e. the hydrostatic distribution of the water pressure is approached. An intermediate point $x^{(D)}$ is introduced in such a way that it divides the grid cell in two unequal segments $\langle x^{(j)}, x^{(D)} \rangle$ and $\langle x^{(D)}, x^{(k)} \rangle$. For a linear potential distribution, the value of $h_{\mathrm{w}}^{(D)}$ would be equal to $h_{\mathrm{w}}^{(B)}$ defined as:

$$h_{\mathrm{w}}^{(B)} = h_{\mathrm{w}}^{(k)} - \frac{\left(\Delta h_{\mathrm{w}}^{(jk)}\right)^2}{\zeta \, \Delta x^{(jk)}} . \tag{4.46}$$

In unsaturated conditions, the value of the potential head $h_{\mathrm{w}}^{(D)}$ should fall between $h_{\mathrm{w}}^{(j)}$ and $h_{\mathrm{w}}^{(B)}$. On the basis of Fig. 4.3 one can assume that the total hydraulic gradient within the segment $\langle x^{(D)}, x^{(j)} \rangle$ is approximately the same as the hydraulic gradient between $x^{(j)}$ and $x^{(k)}$, and both of them are close to zero:

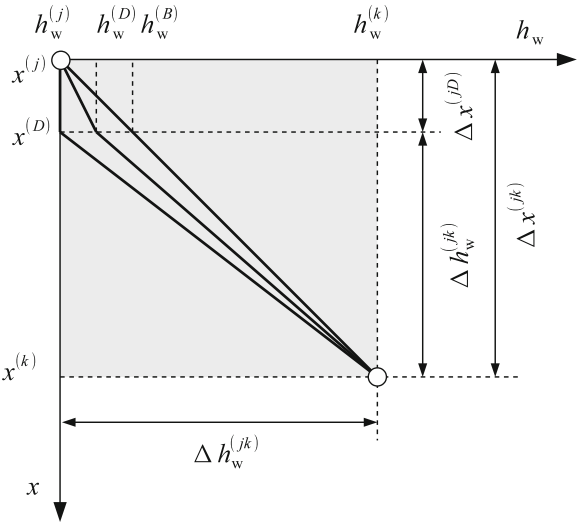

Fig. 4.3 Water potential head profile during drainage close to the hydrostatic state. Modified with permission from [39]

$$\frac{h_w^{(k)} - h_w^{(D)}}{x^{(k)} - x^{(D)}} - \zeta \approx \frac{h_w^{(k)} - h_w^{(j)}}{x^{(k)} - x^{(j)}} - \zeta \to 0 \,. \tag{4.47}$$

On the other hand, for the conditions close to the hydrostatic state the value of the inter-nodal permeability approaches the permeability of the upper node. Thus, the average permeability in the segment $\langle x^{(D)}, x^{(k)} \rangle$ is approximately $k_{rw}^{(Dk)} \approx k_{rw}^{(D)}$. The value of $k_{rw}^{(D)}$ is not known—it is between $k_{rw}^{(j)}$ and $k_{rw}^{(B)}$. Let us assume $k_{rw}^{(D)} \approx k_{rw}^{(B)}$—if one assumes $k_{rw}^{(D)} = k_{rw}^{(j)}$, then the conductivity for the whole grid block would be equal to $k_{rw}^{(j)}$, which is correct only for the limit case when $\Delta h_w^{(jk)} / \Delta x^{(jk)} = \zeta$. Consequently, the water flux between $x^{(D)}$ and $x^{(k)}$ is estimated as:

$$v_w^{(Dk)} \approx -k_{rw}^{(Dk)} \left(\frac{h_w^{(k)} - h_w^{(D)}}{\Delta x^{(jk)} - \Delta x^{(jD)}} - \zeta \right) \approx -k_{rw}^{(B)} \left(\frac{h_w^{(k)} - h_w^{(j)}}{\Delta x^{(jk)}} - \zeta \right) . \tag{4.48}$$

For steady flow, the flux $v_w^{(Dk)}$ should be equal to the average flux between the nodes j and k:

$$v_w^{(Dk)} = v_w^{(jk)} = -k_{rw}^{(jk)} \left(\frac{h_w^{(k)} - h_w^{(j)}}{\Delta x^{(jk)}} - \zeta \right) . \tag{4.49}$$

Therefore, the following approximation can be developed:

$$k_{rw}^{(jk)} \approx k_{rw}^{(B)} \,, \tag{4.50}$$

where:

$$k_{\mathrm{rw}}^{(B)} = k_{\mathrm{rw}}\left(h_{\mathrm{w}}^{(B)}\right) = k_{\mathrm{rw}}\left(h_{\mathrm{w}}^{(k)} - \frac{\left(\Delta h_{\mathrm{w}}^{(jk)}\right)^2}{\zeta\ \Delta x^{(jk)}}\right) \tag{4.51}$$

For $\Delta h_{\mathrm{w}}^{(jk)} \to \Delta x^{(jk)}$, Eq. (4.50) yields the expected limit value $k_{\mathrm{rw}}^{(jk)} \to k_{\mathrm{rw}}^{(j)}$, while for $\Delta h_{\mathrm{w}}^{(jk)} \ll \Delta x^{(jk)}$ the value of the inter-nodal conductivity tends to $k_{\mathrm{rw}}^{(k)}$, which is an overestimation and does not satisfy Eq. (4.45). The suggested approach is to use the minimum of the two values of $k_{\mathrm{rw}}^{(jk)}$ given by Eqs. (4.45) and (4.50):

$$k_{\mathrm{rw}}^{(jk)} = \min\left(k_{\mathrm{rw}}^{(B)}, \frac{\zeta\ k_{\mathrm{rw}}^{(j)}}{\zeta - \Delta h_{\mathrm{w}}^{(jk)}/\Delta x^{(jk)}}\right). \tag{4.52}$$

The obtained averaging formula is very simple to implement, as it does not involve the integrated average.

4.2.3 Capillary Rise

In contrast to the previous cases, for capillary rise the over- or underestimation of the inter-nodal permeability does not lead to oscillations in the numerical solution. While the permeability in the upper part of the domain is smaller than in the lower part, this can be always compensated for by an arbitrarily small potential gradient in the lower part, i.e. the water pressure profile close to hydrostatic, see Fig. 4.4. Therefore, any value of the inter-nodal permeability from the range $k_{\mathrm{rw}}^{(j)}$ to $k_{\mathrm{rw}}^{(k)}$ will lead to physically admissible monotonous solution. Nevertheless, depending on $\Delta x^{(jk)}$, the actual steady-state relative permeability varies from the permeability of the upper node $k_{\mathrm{rw}}^{(j)}$ to the integrated mean $k_{\mathrm{int}}^{(jk)}$, which in the case of initially dry soil may represent a range of several orders of magnitude. A more accurate approximation of $k_{\mathrm{rw}}^{(j)}$ can be obtained if the grid cell is divided in two parts, as shown in Fig. 4.4. The length of the upper sub-cell is denoted by $\Delta x^{(jE)}$, while the length of the lower sub-cell is $\Delta x^{(Ek)}$. The position of point $x^{(E)}$ is chosen in such a way that the corresponding value of the water pressure head is:

$$h_{\mathrm{w}}^{(E)} = h_{\mathrm{w}}^{(k)} - \zeta\ \Delta x^{(jk)}\ . \tag{4.53}$$

In the lower sub-cell, the water pressure distribution is close to the hydrostatic one, which means that the average permeability between the points $x^{(E)}$ and $x^{(k)}$ can be estimated as:

$$k_{\mathrm{rw}}^{(Ek)} \approx k_{\mathrm{rw}}^{(E)} = k_{\mathrm{rw}}\left(h_{\mathrm{w}}^{(E)}\right)\ . \tag{4.54}$$

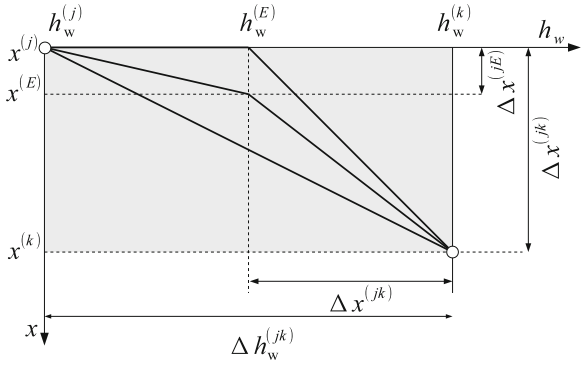

Fig. 4.4 Water pressure head profile for capillary rise. Modified with permission from [39]

In the upper sub-cell, the flow is dominated by capillary forces and the average permeability can be approximated by the integrated mean:

$$k_{\text{int}}^{(jE)} = \frac{1}{h_{\text{w}}^{(E)} - h_{\text{w}}^{(j)}} \int_{h_{\text{w}}^{(j)}}^{h_{\text{w}}^{(E)}} k_{\text{rw}}(\hat{h})\, \mathrm{d}\hat{h} \,. \tag{4.55}$$

For steady-state flow, the water flux should be the same in each part of the cell. Moreover, it should be equal to the flux between nodes j and k estimated using the average inter-nodal permeability $k_{\text{rw}}^{(jk)}$. This conditions can be written as follows:

$$v_{\text{w}}^{(jk)} = v_{\text{w}}^{(jE)} = v_{\text{w}}^{(Ek)} \,, \tag{4.56}$$

where:

$$v_{\text{w}}^{(jk)} = -k_{\text{rw}}^{(jk)} \left(\frac{\Delta h_{\text{w}}^{(jk)}}{\Delta x^{(jk)}} - \zeta \right) , \tag{4.57}$$

$$v_{\text{w}}^{(jE)} = -k_{\text{int}}^{(jE)} \left(\frac{\Delta h_{\text{w}}^{(jk)} - \zeta\, \Delta x^{(jk)}}{\Delta x^{(jE)}} - \zeta \right) , \tag{4.58}$$

$$v_{\text{w}}^{(Ek)} = -k_{\text{rw}}^{(E)} \left(\frac{\zeta\, \Delta x^{(jk)}}{\Delta x^{(jk)} - \Delta x^{(jE)}} - \zeta \right) . \tag{4.59}$$

The double equality (4.56) can be transformed to a system of two equations with two unknowns, $k_{\text{rw}}^{(jk)}$ and $\Delta x^{(jE)}$. By requiring $v_{\text{w}}^{(jE)} = v_{\text{w}}^{(Ek)}$ one arrives at a quadratic equation with respect to $\Delta x^{(jE)}$. This equation has one positive and one negative root. The positive root is given by the following formula:

$$\Delta x^{(jE)} = \frac{-\Delta h_{\mathrm{w}}^{(jk)} + Z_{\mathrm{k}}}{2\,\zeta\,(k_{\mathrm{rw}}^{(E)}/k_{\mathrm{int}}^{(jE)} - 1)}\,, \tag{4.60}$$

where:

$$Z_{\mathrm{k}} = \sqrt{\left(\Delta h_{\mathrm{w}}^{(jk)}\right)^2 + 4\,\zeta\,\Delta x^{(jk)}\,\left(k_{\mathrm{rw}}^{(E)}/k_{\mathrm{int}}^{(jE)} - 1\right)\,\left(\Delta h_{\mathrm{w}}^{(jk)} - \zeta\,\Delta x^{(jk)}\right)}\,. \tag{4.61}$$

The average permeability $k_{\mathrm{rw}}^{(jk)}$ is equal to the weighted harmonic average of the permeabilities of the two sub-cells:

$$k_{\mathrm{rw}}^{(jk)} = \frac{\Delta x^{(jk)}\,k_{\mathrm{int}}^{(jE)}\,k_{\mathrm{rw}}^{(E)}}{(\Delta x^{(jk)} - \Delta x^{(jE)})\,k_{\mathrm{int}}^{(jE)} + \Delta x^{(jE)}\,k_{\mathrm{rw}}^{(E)}}\,. \tag{4.62}$$

Note that the harmonic averaging is applied to the values of $k_{\mathrm{int}}^{(jE)}$ and $k_{\mathrm{rw}}^{(E)}$ which themselves represent average permeabilities and can be considered uniform in the respective parts of the cell. Such an approach is physically justified, in contrast to the harmonic averaging of nodal relative permeabilities $k_{\mathrm{rw}}^{(j)}$ and $k_{\mathrm{rw}}^{(k)}$ as described in Sect. 4.1.1. While the final formula for capillary rise is somewhat more complex than the formulas for infiltration and drainage, the arithmetic operations are straightforward to perform once the value of the integrated mean $k_{\mathrm{int}}^{(jE)}$ is known.

4.2.4 Implementation Issues

The application of the method described above requires that for any pair of nodal values of the pressure head, $h_{\mathrm{w}}^{(j)}$ and $h_{\mathrm{w}}^{(k)}$, first the value of the capillary gradient $\Delta h_{\mathrm{w}}^{(jk)}/\Delta x^{(jk)}$ needs to be computed and compared to the gravity coefficient ζ. Based on this comparison, one of the three available formulae must be chosen. It means that for more complex flow scenarios the averaging formula may change with time and/or spatial position.

While the method was developed for the pressure head as the primary variable in the Richards equation, it can be easily adapted to the case of primary variable p_{w}. To this order the values of pressure head should be replaced by the values of the pressure, while the gravity coefficient ζ should be replaced by $\zeta\,\rho_{\mathrm{w}}\,g$, where g is the magnitude of the gravitational acceleration. In the numerical examples presented below both forms of the governing equations are used.

The proposed approach, similarly to the integrated mean and the method of Baker [3], requires an integration of the relative permeability defined as a function of the water pressure (or pressure head). For several models of the relative permeability functions, including the exponential, Brooks–Corey–Burdine and Brooks–Corey–Mualem models, this can be done analytically. However, for the widely used van Genuchten–Mualem model (and many other), analytical integration

is not possible. The use of numerical integration significantly increases the computational effort and the time of the simulation. An efficient approach is to create at the preprocessing stage a look-up table containing the values of the flux potential Φ_p or Φ_h defined as a function of the water pressure (or head). These values are calculated using numerical integration with a large number of quadrature points, in order to obtain an accurate approximation. During the simulation of unsteady flow, the integrated mean is computed as the difference in flux potentials divided by the difference in the pressures (or heads), with the values of the flux potential interpolated from the look-up table. In the examples presented below, linear interpolation was used, although more sophisticated techniques are also available [30]. Interpolation from a look-up table can be also used to evaluate the water saturation and the relative permeability as functions of the water pressure. Such an approach offers a significant speedup of the computations, even if simple permeability averaging schemes are employed. In order to minimize the error introduced by interpolation, the points should be spaced non-uniformly, with higher density in the regions where the values of hydraulic functions change more rapidly. Numerical experiments presented in [39] and [40] showed that if the interpolation is used, the proposed averaging method requires simulation time comparable to the standard averaging approaches like arithmetic or geometric means.

4.2.5 Evaluation for Steady Flow

The accuracy of the formulae presented in the previous sections can be evaluated by comparing the resulting values of the inter-nodal permeability with the ones obtained from the solution of equation describing steady state incompressible unsaturated flow between two nodes. First, let us consider exponential relative permeability function given by Eq. (4.22). In this case the exact value of the steady-state inter-nodal permeability is given by the formula of Baker et al. [5], Eq. (4.26), which results from the analytical solution of the steady flow equation. In Tables 4.2 and 4.3 these exact permeability values (K-EXACT) are compared with the approximations obtained using the formulae of Szymkiewicz [39] (K-SZYM), described in Sects. 4.2.1–4.2.3, as well as other commonly used averaging schemes. They include the arithmetic (K-ARIT), geometric (K-GEOM), harmonic (K-HARM) and integrated (K-INT) averages, as well as upstream weighting (K-UPS) and the method based of flux splitting (K-SPLIT), as given by Eqs. (4.14) and (4.17). In the latter case, it was assumed that the relative permeability for the capillary flux is equal to the integrated mean approach and the relative permeability for the gravitational flux is equal to the permeability of the upper node. The calculations were carried out for two values of the pressure scaling parameter: $h_g = 1\,\mathrm{m}$ and $h_g = 0.05\,\mathrm{m}$, which correspond respectively to a moderate and a strong nonlinearity in the $k_{rw}(h_w)$ relationship. Two values of the gravity coefficient were used: $\zeta = 1$ (vertical flow) and $\zeta = 0.707$ (flow direction inclined by 45° to the horizontal plane). The inter-nodal distance was assumed constant, $\Delta x = 0.2\,\mathrm{m}$. A number of boundary value problems were

Table 4.2 Exact and approximate steady-state inter-nodal permeability values for exponential relative permeability function with $h_g = 1$ m, $\Delta x = 0.2$ m

Test case	1	2	3	4	5	6
Flow type	Infiltration	Capillary rise	Drainage	Infiltration	Capillary rise	Drainage
$h_w^{(j)}$ (m)	−1.00E−03	−5.00E+00	−1.50E−01	−1.00E−03	−5.00E+00	−1.00E−01
$k_{rw}^{(j)}$ (–)	9.99E−01	6.74E−03	8.61E−01	9.99E−01	6.74E−03	9.05E−01
$h_w^{(k)}$ (m)	−5.00E+00	−1.00E−03	−1.00E−03	−5.00E+00	−1.00E−03	−1.00E−03
$k_{rw}^{(k)}$ (–)	6.74E−03	9.99E−01	9.99E−01	6.74E−03	9.99E−01	9.99E−01
ζ (–)	1.00E+00	1.00E+00	1.00E+00	7.07E−01	7.07E−01	7.07E−01
K-EXACT	2.11E−01	1.86E−01	9.26E−01	2.07E−01	1.90E−01	9.50E−01
K-SZYM	1.98E−01	1.92E−01	8.94E−01	1.98E−01	2.00E−01	9.32E−01
K-ARIT	5.03E−01	5.03E−01	9.30E−01	5.03E−01	5.03E−01	9.52E−01
K-GEOM	8.20E−02	8.20E−02	9.27E−01	8.20E−02	8.20E−02	9.51E−01
K-HARM	1.34E−02	1.34E−02	9.25E−01	1.34E−02	1.34E−02	9.50E−01
K-INT	1.98E−01	1.98E−01	9.28E−01	1.98E−01	1.98E−01	9.51E−01
K-UPS	9.99E−01	9.99E−01	8.61E−01	9.99E−01	9.99E−01	9.05E−01
K-SPLIT	2.29E−01	2.06E−01	6.64E−01	2.21E−01	2.04E−01	7.97E−01

Table 4.3 Exact and approximate steady-state inter-nodal permeability values for exponential relative permeability function with $h_g = 0.05$ m, $\Delta x = 0.2$ m

Test case	7	8	9	10	11	12
Flow type	Infiltration	Capillary rise	Drainage	Infiltration	Capillary rise	Drainage
$h_w^{(j)}$ (m)	−1.00E−03	−5.00E+00	−1.50E−01	−1.00E−03	−5.00E+00	−1.00E−01
$k_{rw}^{(j)}$ (–)	9.80E−01	3.72E−44	4.98E−02	9.80E−01	3.72E−44	1.35E−01
$h_w^{(k)}$ (m)	−5.00E+00	−1.00E−03	−1.00E−03	−5.00E+00	−1.00E−03	−1.00E−03
$k_{rw}^{(k)}$ (–)	3.72E−44	9.80E−01	9.80E−01	3.72E−44	9.80E−01	9.80E−01
ζ (–)	1.00E+00	1.00E+00	1.00E+00	7.07E−01	7.07E−01	7.07E−01
K-EXACT	3.84E−02	7.62E−04	1.27E−01	2.87E−02	1.79E−03	2.74E−01
K-SZYM	3.77E−02	4.74E−04	1.06E−01	2.70E−02	1.51E−03	2.45E−01
K-ARIT	4.90E−01	4.90E−01	5.15E−01	4.90E−01	4.90E−01	5.58E−01
K-GEOM	1.91E−22	1.91E−22	2.21E−01	1.91E−22	1.91E−22	3.64E−01
K-HARM	7.44E−44	7.44E−44	9.38E−02	7.44E−44	7.44E−44	2.38E−01
K-INT	9.80E−03	9.80E−03	3.12E−01	9.80E−03	9.80E−03	4.27E−01
K-UPS	9.80E−01	9.80E−01	4.98E−02	9.80E−01	9.80E−01	1.35E−01
K-SPLIT	4.71E−02	1.02E−02	−7.17E−01	3.65E−02	1.01E−02	−5.45E−01

examined, which represent all three types of flow, i.e. infiltration, drainage and capillary rise in either vertical or inclined direction.

It can be seen that the approximation method proposed by the author (K-SZYM) is in most cases more accurate than any other method. The exceptions are represented by test cases 3 and 6, corresponding to drainage where the permeabilities at the upper and lower node are very similar, and consequently most of the averaging methods give similar results. It should be noted that for the same two cases the method based on flux splitting predicts average permeability which is outside the range of values defined

by the two nodal permeabilities, and thus physically inadmissible. It means that such an averaging scheme should be used with care. The advantages of the new method can be seen even more clearly in Table 4.3, where the results for highly nonlinear relative permeability function are reported. Here the maximum relative error of the new method does not exceed 40 %, while other methods often lead to errors of more than one order of magnitude. For drainage (test cases 9 and 12) the method based on flux splitting predicts negative values of the permeability coefficient, which means that the flux direction is opposite to the direction resulting from the water potential gradient.

Further results for steady-state flow can be found in [39]. In that paper various averaging schemes were verified against numerical solutions of steady flow equation for fifteen relative permeability functions, corresponding to a range of soils from sands to clays. Included were four Brooks–Corey–Burdine functions, four van Genuchten–Mualem functions, two exponential functions, one Gardner function, two van Genuchten–Mualem functions with negative connectivity parameter κ (see Sect. 2.1.6), and two combinations of van Genuchten capillary function with power-type relative permeability functions, as proposed in [27]. For each function a large number of steady flow problems was solved, with the internodal distances varying between 1 mm and 100 m and the nodal values of the water pressure head ranging from -1 mm to -100 m. For any specific test case, the error of the considered averaging scheme was defined as follows:

$$\text{ERR-K} = \log_{10} \frac{k_{\text{rw}}^{(jk)}}{k_{\text{ref}}^{(jk)}} \tag{4.63}$$

where $k_{\text{rw}}^{(jk)}$ was computed with the considered averaging scheme, and $k_{\text{ref}}^{(jk)}$ is the reference value obtained from the numerical solution of steady state flow equation between nodes. Such a formulation was chosen in order to give equal weight to over- and underestimation of the average permeability, and to facilitate comparison of the relative errors, which often differ by several orders of magnitude. In view of the large number of results, representative error measures were defined to quantify the accuracy of each method of inter-nodal permeability approximation:

- root-mean square error, RMS-ERR-K

$$\text{RMS-ERR-K} = \sqrt{\frac{1}{N} \sum_{1}^{N} (\text{ERR-K})^2} \tag{4.64}$$

  where N is the number of test cases in the considered set,
- maximum error value (largest overestimation), max(ERR-K),
- minimum error value (largest underestimation), min(ERR-K).

The values of these error measures are reported in Table 4.4 for some of the averaging methods used in the previous example: K-ARIT, K-GEOM, K-INT, K-UPS

Table 4.4 Root-mean-square errors obtained with various permeability averaging schemes for steady flow test cases. Data from [39]

	K-SZYM	K-BAKER	K-GASTO	K-ARIT	K-GEOM	K-INT	K-UPS
Average	0.12	0.36	0.29	1.61	1.14	1.01	1.30
Small Δx	0.04	0.07	0.33	1.13	0.84	0.09	1.34
Medium Δx	0.13	0.38	0.22	1.33	0.89	0.62	1.44
Large Δx	0.17	0.49	0.19	2.17	1.55	1.68	1.10
Infiltration	0.04	0.11	0.33	0.86	1.26	0.57	1.04
Drainage	0.22	0.51	0.09	2.57	1.29	1.90	0.27
Capillary rise	0.11	0.49	0.26	1.74	0.77	0.64	1.96

and K-SZYM. Moreover, computations were performed with the method of [19] (K-GASTO), for Brooks–Corey and van Genuchten–Mualem functions and node spacing satisfying condition given by Eq. (4.36), and with the method of Baker [3] (K-BAKER), for those relative permeability functions, which can be inverted analytically to obtain $h_{\mathrm{w}}(k_{\mathrm{rw}})$.

Table 4.4 provides the average value of RMS-ERR-K for all test cases, as well as separate results obtained for three ranges of inter-nodal distances Δx: small (1 mm, 1 cm, 2 cm), medium (10, 20, 50 cm) and large (1, 10, 100 m), and three types of flow (infiltration, drainage, capillary rise). It should be noted that due to its definition RMS-ERR-K is always positive and provides information only on the magnitude of error, without indicating whether the specific method under- or overestimates the internodal permeability. As the errors are defined in terms of decimal logarithm, a value of RMS-ERR-K $= 1.0$ corresponds to an error of one order of magnitude (i.e. 1000 %), while a value of 0.17—to an error of about 50 %.

Overall, it can be seen that the methods based on Darcian means are significantly more accurate than the simple averaging schemes, especially on medium or coarse grids. On fine grids, accurate results were obtained also with the integrated mean approach. As far as the type of flow is considered, the author's method gave the best results of all methods for infiltration and capillary rise, while for drainage it was second best, after the method of Gasto et al. [19]. The performance of the simple methods differ significantly, depending on the type of flow. For infiltration, the arithmetic and integrated averages provided average errors below one order of magnitude, while the average errors of the geometric average and the upstream weighting exceeded this value. In contrast, for drainage the upstream weighting largely outperformed the other simple methods, allowing to obtain very high accuracy. For the capillary rise, the geometric and integrated means proved more accurate than the arithmetic and upstream means.

Finally, the methods can be also compared in terms of the largest error obtained for the ensemble of test problems. The maximum and minimum error values are reported in Table 4.5. The most extreme case corresponds to the overestimation of the inter-nodal permeability by 10.5 orders of magnitude using the arithmetic mean approach, which occurred for drainage with large Δx in a soil characterized by a very rapid decrease of the relative permeability within a small range of the negative

Table 4.5 Root-mean-square errors obtained with various permeability averaging schemes for steady flow test cases. Data from [39]

	K-SZYM	K-BAKER	K-GASTO	K-ARIT	K-GEOM	K-INT	K-UPS
min(ERR-K)	−1.50	−4.30	−1.24	−2.89	−5.38	−3.23	−6.05
max(ERR-K)	0.11	4.47	1.60	10.50	5.40	8.55	8.18

values of the water pressure head. Other simple averaging methods may also lead to over- or underestimation of the permeability by several orders of magnitude in particular conditions. Significant errors were generated also by the method of Baker [3], despite the fact that the average errors obtained with this method are rather small. This indicates that the latter method may be relatively inaccurate for some specific types of the relative permeability functions. In contrast, the largest errors generated by the method of Szymkiewicz [39] did not exceed 1.5 order of magnitude. The method of Gasto et al. [19] was similarly accurate, but due to its limitations it could be applied to a substantially smaller number of test cases.

4.2.6 Evaluation for Unsteady Flow

In this section, four one-dimensional unsteady flow test cases are discussed, in order to show the performance of the proposed method in comparison with other averaging schemes. The first two examples are similar to the ones presented in [39], but differ in the values of soil parameters and in accounting for the compressibility of water. The soil is characterized by Brooks–Corey–Burdine hydraulic functions with the following parameters: porosity $\phi = 0.4$, residual saturations $S_{\mathrm{rw}} = S_{\mathrm{ra}} = 0$, intrinsic permeability $k_{\mathrm{s}} = 8.5 \times 10^{-12}\,\mathrm{m}^2$, entry pressure $p_{\mathrm{e}} = 440\,\mathrm{Pa}$, exponent $n_{\mathrm{b}} = 1.124$. The parameters correspond to sand with a relatively uniform grain size distribution.

The first example is vertical downward infiltration in a 2-m thick soil layer with initially uniform distribution of the water pressure $p_{\mathrm{w}} = -49050\,\mathrm{Pa}$, corresponding to the water saturation of 0.005. At the soil surface a constant value of the water pressure is imposed, $p_{\mathrm{w}} = -500\,\mathrm{Pa}$ ($S_{\mathrm{w}} = 0.866$), while at the bottom of the layer the free drainage condition is applied. Numerical simulations were performed for two values of node spacing, $\Delta x = 20\,\mathrm{cm}$ and $\Delta x = 1\,\mathrm{cm}$, respectively. Figure 4.5 shows the water saturation profiles after 3 h of infiltration obtained on the coarser grid for various permeability averaging schemes. They are compared to the reference solution obtained on a fine grid with $\Delta x = 1\,\mathrm{mm}$. For such a fine discretization, essentially the same results were obtained using K-INT and K-UPS schemes. As discussed above, these two averaging schemes represent the limit values of the inter-nodal conductivity for downward infiltration. Thus, the corresponding solution is assumed to be a close approximation of the exact solution. The reference solution predicts a very sharp wetting front, which cannot be exactly reproduced on the coarse grid. However, K-UPS, K-ARIT, K-BAKER and K-SZYM approximate the position of the wetting front with reasonable accuracy. The latter two methods give very similar

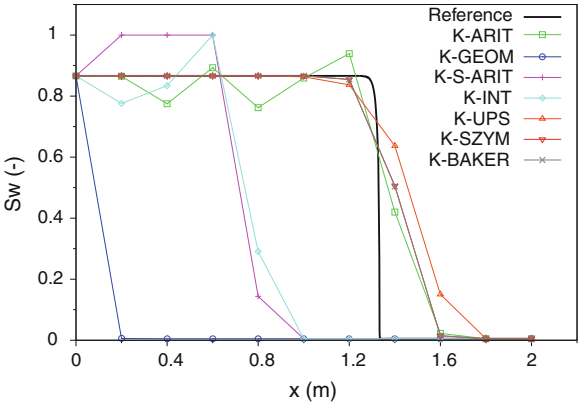

Fig. 4.5 Example 1: water saturation profiles obtained with various permeability averaging methods, coarse grid

results, which are somewhat more accurate than the upstream weighting and on the other hand do not produce oscillations, which occur in the solution obtained with K-ARIT. The integrated mean (K-INT) and the method based on arithmetic averaging of the water saturation (K-S-ARIT) not only lead to oscillations but also considerably underestimate the position of the wetting front. The least accurate solution is given by the geometric mean, which severely underestimates the inter-nodal permeability and consequently predicts virtually no flow. The latter three methods are clearly not adequate to simulate gravity-dominated infiltration on coarse grids.

In contrast, if a finer node spacing of 1 cm is used, the differences between various methods are much smaller. The only exception is the geometric mean, which still underestimates the position of the wetting front and produces saturation values larger than the boundary saturation in the wet zone (not shown here). In order to better show the differences between the other methods, only a small part of the solution domain near the wetting front is presented in Fig. 4.6. For the considered node spacing, K-SZYM gives the same values as K-INT (the latter one is not shown in the figure). This approach underestimates the position of the wetting front, albeit only slightly. Even better results are obtained with K-BAKER, K-GASTO and K-S-ARIT. In contrast, both K-ARIT and K-UPS give more diffuse solutions, which overestimate the position of the wetting front, K-UPS being less accurate than K-ARIT. Note also that the geometric averaging predicts the position of the wetting front at the value of $x \approx 0.5\,\mathrm{m}$, well outside the range shown in the figure.

The second example concerns drainage in the same domain as in Example 1. The initial condition is $p_\mathrm{w} = 0$ in the whole soil layer and this value is maintained at the bottom as the boundary condition. At the soil surface a zero-flux condition is imposed. Water drains from the layer under the influence of gravity. The same values of Δx as in Example 1 were used. The water saturation profiles for coarse grid after 4 h of drainage are shown in Fig. 4.7. It can be seen that all simple permeability averaging

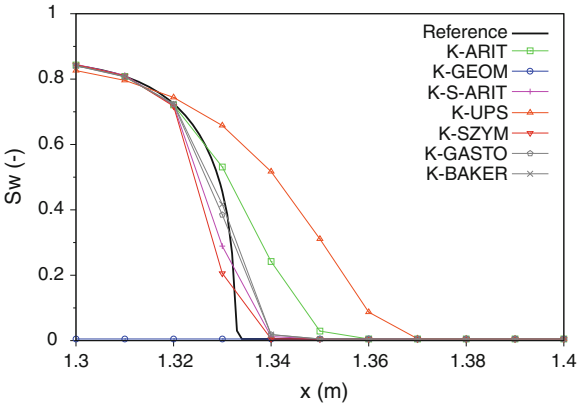

Fig. 4.6 Example 1: water saturation profiles obtained with various permeability averaging methods, fine grid

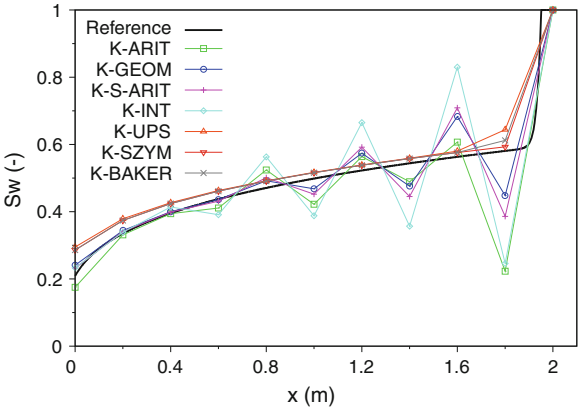

Fig. 4.7 Example 2: water saturation profiles obtained with various permeability averaging methods, coarse grid

schemes lead to oscillatory solutions. In contrast, monotonous saturation profiles are obtained with K-UPS, K-BAKER and K-SZYM, the latter one being closest to the reference solution. For the finer grid, $\Delta x = 1$ cm, all averaging schemes produce very accurate solutions, thus the results are not shown here.

The test cases presented above may suggest that the node spacing of about 1 cm is fine enough to obtain sufficiently accurate results with the arithmetic averaging scheme, which is widely used in unsaturated flow modelling. Such a conclusion was drawn by van Dam and Feddes [43] on the basis of several numerical simulations performed by those authors. However, a re-examination of two of their test cases presented by Szymkiewicz [39] showed that the results obtained with $\Delta x = 1$ cm significantly differ from those obtained for a finer grid if arithmetic averaging is

applied. The two cases (Examples 3 and 4 in the numeration of this chapter) are briefly described here, following [39]. Both problems concern vertical flow in a 40 cm column of soil characterized by the van Genuchten capillary function and Mualem relative permeability function with the following parameters: $\theta_{sw} = 0.43$, $\theta_{rw} = 0.01$, $p_g = 3940\,\text{Pa}$, $n_g = 1.507$, $m_g = 1 - 1/n_g$, $k_s = 2.065 \times 10^{-13}\,\text{m}^2$ ($K_{sw} = 17.5\,\text{cm}\,\text{d}^{-1}$) and the connectivity parameter $\kappa = -0.14$. Note that for the non-standard Mualem permeability function neither K-GASTO nor K-BAKER can be applied.

The boundary conditions correspond to the soil–atmosphere interface, as described in Sect. 2.3.2. In Example 3 the soil is initially dry, with a uniform water content $\theta_w^{init} = 0.1$, corresponding to the water pressure head $h_w^{init} = -832.5\,\text{cm}$. At the top of the column a constant infiltration flux of $v_w^{top} = 100\,\text{cm}\,\text{d}^{-1}$ is imposed, until the soil surface reaches saturation. Afterwards, the boundary condition is switched to a constant pressure head, $h_w^{top} = 0$. The infiltration continues, but the value of the flux decreases in time. At the bottom, the initial value of the water content is maintained. The solutions are compared in terms of the cumulative infiltration q_{inf}, defined as the integral of the infiltration flux over time. The reference solution obtained on a fine grid with $\Delta x = 0.05\,\text{cm}$ predicted the cumulative infiltration of $q_{inf} = 3.69\,\text{cm}$ at $t = 0.1\,\text{d}$, while the ponding occured (the surface became saturated) at $t_{pond} = 0.006\,\text{day}$. On such a fine grid, virtually the same results were obtained using the arithmetic and integrated permability averaging and they were cross-checked with the Hydrus-1D code [35]. On a coarser grid of $\Delta x = 1\,\text{cm}$, the arithmetic averaging yielded the cumulative infiltration $q_{inf} = 3.88\,\text{cm}$ and $t_{pond} = 0.009\,\text{d}$, the geometric averaging: $q_{inf} = 3.66\,\text{cm}$ and $t_{pond} = 0.002\,\text{d}$, respectively, while the author's method: $q_{inf} = 3.68\,\text{cm}$ and $t_{pond} = 0.006$ d. In this case the new method offers a considerable improvement over the arithmetic averaging.

In Example 4 the soil is initially moderately wet ($\theta_w^{init} = 0.1$, $h_w^{init} = -200\,\text{cm}$) and a constant evaporation flux of $v_w^{top} = -0.5\,\text{cm}\,\text{d}^{-1}$ is applied at the surface, until the water pressure head at the surface reaches the value of $h_{dry} = -1377\,\text{m}$, which is then maintained as a Dirichlet boundary condition. The evaporation continues, but the flux diminishes with time. At the bottom, the initial value of the water pressure head is kept. Similarly to the previous case, the solutions are compared in terms of the cumulative flux at the surface. According to the reference solution ($\Delta x = 0.05\,\text{cm}$), the cumulative evaporation flux after 5 days is $q_{ev} = 0.89\,\text{cm}$ and the water pressure head at the soil surface reaches its limit value after $t_{dry} = 0.51$ day. For $\Delta x = 1\,\text{cm}$ the differences between averaging schemes are even larger than in the previous case, with the arithmetic averaging predicting $q_{ev} = 1.12\,\text{cm}$ and $t_{dry} = 1.14\,\text{d}$, the upstream averaging: $q_{ev} = 1.26\,\text{cm}$ and $t_{dry} = 1.41\,\text{d}$, and the author's method: $q_{ev} = 0.90\,\text{cm}$ and $t_{dry} = 0.63\,\text{d}$. Again, the new method proved more accurate than the arithmetic mean.

4.3 Saturated–Unsaturated Transition

A special case for permeability averaging arises when one of the nodes is fully water-saturated, with the water pressure larger than the entry pressure for the given soil, while the other node is unsaturated. If the value of the water pressure at the saturated node increases, the inter-nodal relative permeability obtained from the steady-state solution will also increase, tending in the limit to the value $k_{\mathrm{rw}}^{(\mathrm{jk})} = 1$. Among the simple averaging methods presented in Sect. 4.1, only the integrated mean, Eq. (4.9), and the formula based on the arithmetic average of nodal pressures, Eq. (4.8), are able to reproduce this behaviour. Other methods, based on the averaging of the nodal permeabilities or saturations, do not predict any change in the inter-nodal permeability, because both permeability and saturation are independent of the water pressure in the saturated range. For a more detailed discussion of the errors arising at the saturated–unsaturated interface, see [31].

As far as the methods based on the Darcian averaging approach are considered, one should note that the formulae presented in Sect. 4.2 are applicable without any modifications to the case of saturated–unsaturated transition. They are based on the integrated mean permeability and on the values of permeability calculated for some intermediate values of the pressure head. Thus, a change of the pressure head at the saturated node will influence the resulting inter-nodal permeability, even if both nodal permeabilities remain constant. The same is true for the formulae of Baker [2], Baker et al. [5] and Baker [3]. In contrast, the formula of Gasto et al. [19] was developed for strictly unsaturated conditions, but the authors proposed a modification to account for the saturated–unsaturated transition, which can be also used with any other scheme for unsaturated permeability averaging. The grid cell is explicitly divided in two parts, one fully saturated and the other one unsaturated, with the interface located at $x^{(S)}$, as shown in Fig. 4.8. Assuming that node j is saturated, one can write the flux continuity condition at the saturated–unsaturated interface as follows:

$$-k_{\mathrm{rw}}^{(jS)}\left(\frac{h_{\mathrm{w}}^{(S)}-h_{\mathrm{w}}^{(j)}}{\Delta x^{(jS)}}-\zeta\right)=-k_{\mathrm{rw}}^{(Sk)}\left(\frac{h_{\mathrm{w}}^{(k)}-h_{\mathrm{w}}^{(S)}}{\Delta x^{(Sk)}}-\zeta\right), \tag{4.65}$$

where $h_{\mathrm{w}}^{(S)}$ is the water pressure head corresponding to the transition from unsaturated to saturated state (equal to zero or the air entry pressure, depending on the assumed constitutive relationship). The relative permeability in the saturated zone is $k_{\mathrm{rw}}^{(jS)} = 1$, while the permeability in the unsaturated zone $k_{\mathrm{rw}}^{(Sk)}$ can be computed with the formula of Gasto et al. [19], or any other formula suitable for unsaturated flow. If $k_{\mathrm{rw}}^{(Sk)}$ depends on $\Delta x^{(Sk)}$, Eq. (4.65) is nonlinear with respect to $\Delta x^{(Sk)}$ and has to be solved iteratively. A further simplification can be introduced if one considers that the pressure distribution between nodes j and k is linear. This leads to the following expression for the inter-nodal permeability $k_{\mathrm{rw}}^{(jk)}$ [19]:

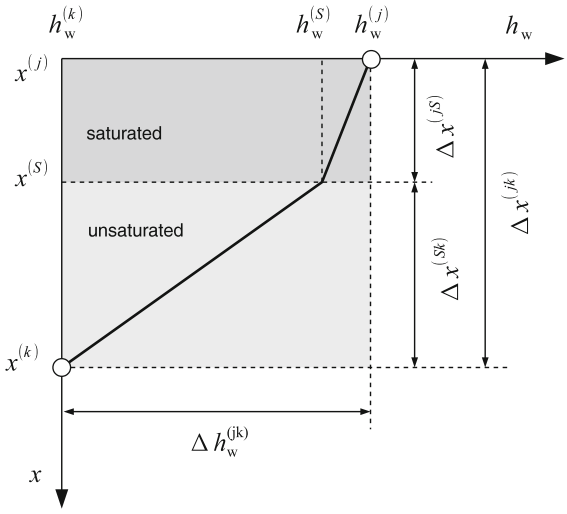

Fig. 4.8 Water pressure head profile near the saturated–unsaturated interface

$$k_{rw}^{(jk)} = \frac{k_{rw}^{(Sk)}\,\Delta h_w^{(jk)}}{\left(h_w^{(k)} - h_w^{(S)}\right) + k_{rw}^{(Sk)}\,\left(h_w^{(S)} - h_w^{(j)}\right)}\,, \tag{4.66}$$

where the unsaturated permeability $k_{rw}^{(Sk)}$ is computed assuming the position of the interface:

$$x^{(S)} = x^{(k)} - \Delta x^{(jk)}\,\frac{h_w^{(k)} - h_w^{(S)}}{\Delta h_w^{(jk)}}\,. \tag{4.67}$$

An analogous formula can be easily obtained for the opposite case, i.e. when the lower node is saturated.

As an example, let us consider steady-state vertical downward flow ($\zeta = 1$) in a porous medium characterized by Brooks–Corey–Burdine relative permeability function with the air-entry pressure head $h_e = 0.25\,\text{m}$ and the shape parameter $n_b = 2.0$. The distance between nodes is $\Delta x = 0.20\,\text{m}$ and the water pressure head at the lower node is $h^{(k)} = -5.0\,\text{m}$, with the corresponding relative permeability $k_{rw}^{(k)} = 3.91 \times 10^{-11}$. At the upper node, the water pressure head assumes four different values, such that $h_w^{(j)} \geq -h_e$ and $k_{rw}^{(j)} = 1$, as shown in Table 4.6. For each case, the inter-nodal relative permeability obtained from a numerical solution of the steady-state problem is compared with four approximations. The approximate methods include those proposed by Szymkiewicz [39] (K-SZYM), Baker et al. [5] (K-BAKER) and Gasto et al. [19] (K-GASTO), as well as the integrated mean (K-INT) and the method based on the arithmetic average of the water pressure head (K-H-ARIT). The results in Table 4.6 shows that the most accurate approximation in this case is obtained with the formula of Baker et al. [5]. Good results are also obtained with K-SZYM, which predicts values equal to the integrated mean, except for the first

Table 4.6 Inter-nodal permeability values for saturated–unsaturated transition obtained from the numerical solution of steady flow equation and various approximating formulae

Test case	1	2	3	4
$h_{\mathrm{w}}^{(j)}$ (m)	−0.25	0.00	1.00	5.00
K-NUM	4.04E−02	9.24E−02	2.42E−01	5.44E−01
K-SZYM	4.04E−02	5.71E−02	2.14E−01	5.29E−01
K-BAKER	4.10E−02	8.89E−02	2.41E−01	5.44E−01
K-GASTO	8.82E−02	9.24E−02	1.09E−01	1.61E−01
K-INT	7.52E−03	5.71E−02	2.14E−01	5.29E−01
K-H-ARIT	6.77E−09	1.00E−08	5.96E−08	1.00E+00

case, where it is close to the reference value, while K-INT underestimates the steady-state permeability by a factor of about 5. K-GASTO is the most accurate method for $h_{\mathrm{w}} = 0$, while in other cases it is less accurate than K-BAKER and K-SZYM, but still correctly reproduces the order of magnitude of the inter-nodal permeability. Finally, the arithmetic averaging of the water pressure head, K-H-ARIT, while showing the expected increase of the inter-nodal permeability with the increase of the pressure at the upper node, leads to very inaccurate results for all cases except the last one, where at least the correct order of magnitude is reproduced.

4.4 Heterogeneous Medium

The permeability averaging methods described in the previous sections were based on the assumption that the porous medium between the two adjacent nodes is homogeneous. Nevertheless, they can be directly applied also for heterogeneous media if the material properties are associated with grid cells (elements) and the nodes are placed at material interfaces (vertex-centred scheme with element-oriented material properties, discussed in Sect. 3.2.4). In such a case, the porous medium between two adjacent nodes is always homogeneous, and any of the averaging methods described above can be applied.

On the other hand, additional considerations are necessary if the adjacent nodes belong to different material regions, as shown in Fig. 4.9. In such a case, physically consistent approximation of the inter-nodal permeability can be obtained if one makes use of the interface conditions discussed in Sect. 2.3.3. The following discussion focuses again on the case of one-dimensional incompressible unsaturated flow. The interface separating materials *I* and *II* is located at $x^{(F)}$, between nodes $x^{(j)}$ and $x^{(k)}$, as shown in Fig. 4.9. The materials are characterized by the saturated hydraulic conductivities K_{sw}^{I} and K_{sw}^{II} and the relative permeability functions $k_{\mathrm{rw}}^{I}(h_{\mathrm{w}})$ and $k_{\mathrm{rw}}^{II}(h_{\mathrm{w}})$, respectively. The flux continuity condition for the interface can be written as follows:

$$v_{\mathrm{w}}^{(jF)} = v_{\mathrm{w}}^{(Fk)} \,, \tag{4.68}$$

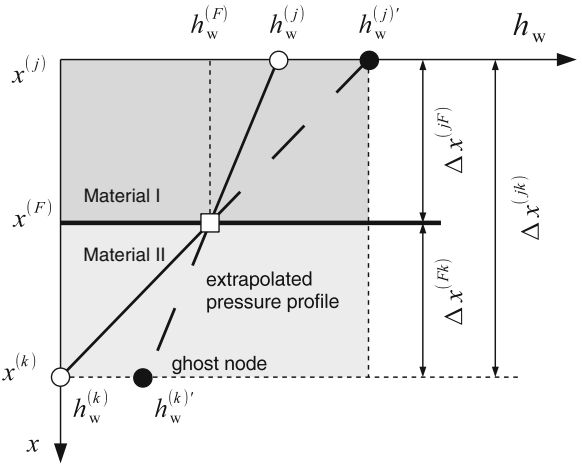

Fig. 4.9 Water pressure head profile in a layered medium. Modified with permission from [40]

where:

$$v_w^{(jF)} = -K_{sw}^{I} \, k_{rw}^{I(jF)} \left[\frac{h_w^{(F)} - h_w^{(j)}}{\Delta x^{(jF)}} - \zeta \right], \tag{4.69}$$

$$v_w^{(Fk)} = -K_{sw}^{II} \, k_{rw}^{II(Fk)} \left[\frac{h_w^{(k)} - h_w^{(F)}}{\Delta x^{(Fk)}} - \zeta \right]. \tag{4.70}$$

In the above equations, $k_{rw}^{I(jF)}$ denotes the average relative permeability in material *I* between node *j* and the interface, while $k_{rw}^{II(Fk)}$ is the average relative permeability in material *II* between the interface and node *k*. Equations (4.68)–(4.70) account for the continuity of the water pressure across the interface since the same value of $h_w^{(F)}$ is used for both sides. The average relative permeabilities for the two layers above and below the interface can be computed with any suitable method, leading to a nonlinear equation with respect to $h_w^{(F)}$. The equation can be solved iteratively, yielding the value of $h_w^{(F)}$ and the corresponding permeabilities in each of the two the sub-cells. The resulting value of the inter-nodal conductivity $K_w^{(jk)}$ must satisfy the following relationship:

$$-K_w^{(jk)} \left[\frac{h_w^{(k)} - h_w^{(j)}}{\Delta x^{(jk)}} - \zeta \right] = v_w^{(jF)} = v_w^{(Fk)} . \tag{4.71}$$

In contrast to the case of homogeneous medium with constant saturated conductivity, here the averaging is applied to the total conductivity $K_w = K_{sw} \, k_{rw}$, not only to the relative permeability k_{rw}. In view of the flux continuity condition given by Eqs. (4.68)–(4.70), the average inter-nodal conductivity $K_w^{(jk)}$ can be subsequently computed the as weighted harmonic mean of the two sub-cell conductivities:

$$K_{\mathrm{w}}^{(jk)} = \left[\Delta x^{(jF)} + \Delta x^{(Fk)}\right] \left[\frac{\Delta x^{(jF)}}{K_{\mathrm{sw}}^{I}\, k_{\mathrm{rw}}^{I(jF)}} + \frac{\Delta x^{(Fk)}}{K_{\mathrm{sw}}^{II}\, k_{\mathrm{rw}}^{II(Fk)}}\right]^{-1} . \tag{4.72}$$

It is clear that the choice of the method used to compute the average relative permeability in each of the homogeneous sub-cells will have significant influence on the final result. Therefore, the use of improved methods based on the Darcian averaging principle is recommended. Note also that for saturated flow, when the relative permeabilities are equal to unity at both sides of the interface, one recovers from Eq. (4.72) a formula for the average saturated conductivity analogous to Eq. (2.110):

$$K_{\mathrm{sw}}^{(jk)} = \left[\Delta x^{(jF)} + \Delta x^{(Fk)}\right] \left[\frac{\Delta x^{(jF)}}{K_{\mathrm{sw}}^{I}} + \frac{\Delta x^{(Fk)}}{K_{\mathrm{sw}}^{II}}\right]^{-1} . \tag{4.73}$$

A number of other methods to calculate inter-nodal permeability at a material interface can be found in the literature. Possibly the most straightforward option is to apply one of the simple averages defined by Eqs. (4.4)–(4.6) to the total conductivity K_{w} or permeability k_{w}, instead of the relative permeability k_{rw}. For the case of arithmetic averaging, the resulting formula can be written as follows:

$$K_{\mathrm{w}}^{(jk)} = \frac{1}{2}\left(K_{\mathrm{sw}}^{I}\, k_{\mathrm{rw}}^{I(j)} + K_{\mathrm{sw}}^{II}\, k_{\mathrm{rw}}^{II(k)}\right) . \tag{4.74}$$

This formula is used, for example, in the well known HYDRUS-1D numerical code [35]. Its drawback is that it does not lead to physically consistent inter-nodal permeability for steady-state saturated flow. In the latter case, as it was mentioned above, accurate results are obtained using the harmonic mean. Therefore, an often used approach, e.g. [1, 13, 26], is to compute the average intrinsic permeability (or saturated conductivity) as the harmonic mean of the intrinsic permeabilities (or saturated conductivities) of the two materials, while the relative permeability is computed by the upstream weighting:

$$K_{\mathrm{w}}^{(jk)} = K_{\mathrm{sw}}^{(jk)}\, k_{\mathrm{rw}}^{(jk)} , \tag{4.75}$$

$$k_{\mathrm{rw}}^{(jk)} = \begin{cases} k_{\mathrm{rw}}^{(j)} & \text{if} \quad \dfrac{h_{\mathrm{w}}^{(k)} - h_{\mathrm{w}}^{(j)}}{\Delta x^{(jk)}} - \zeta \le 0 , \\ k_{\mathrm{rw}}^{(k)} & \text{if} \quad \dfrac{h_{\mathrm{w}}^{(k)} - h_{\mathrm{w}}^{(j)}}{\Delta x^{(jk)}} - \zeta > 0 , \end{cases} \tag{4.76}$$

where $K_{\mathrm{sw}}^{(jk)}$ is given by Eq. (4.73) This method leads to physically consistent result for saturated flow. On the other hand, the use of upstream averaging ensures a monotonous solution.

The scheme proposed by Romano et al. [32] is based on Eq. (4.68) but introduces two additional ghost points in the vicinity of the interface, Fig. 4.9. One of them is located above the interface and extrapolates the pressure profile from the lower layer.

The other one is positioned below the interface and extrapolates the pressure profile from the upper layer. It is assumed that the interface is located mid-way between the nodes j and k and the extrapolation is linear, so the following relation holds:

$$\frac{1}{2}\left(h_{\mathrm{w}}^{(j)} + h_{\mathrm{w}}^{(k)'}\right) = \frac{1}{2}\left(h_{\mathrm{w}}^{(j)'} + h_{\mathrm{w}}^{(k)}\right) , \tag{4.77}$$

where $h_{\mathrm{w}}^{(j)'}$ and $h_{\mathrm{w}}^{(k)'}$ denote the water pressure head values at the ghost nodes. The flux continuity condition is written as:

$$-K_{\mathrm{sw}}^{I}\, k_{\mathrm{rw}}^{I(jk)} \left[\frac{h_{\mathrm{w}}^{(k)'} - h_{\mathrm{w}}^{(j)}}{\Delta x^{(jk)}} - \zeta\right] = -K_{\mathrm{sw}}^{II}\, k_{\mathrm{rw}}^{II(jk)} \left[\frac{h_{\mathrm{w}}^{(k)} - h_{\mathrm{w}}^{(j)'}}{\Delta x^{(jk)}} - \zeta\right] , \tag{4.78}$$

where the average relative permeability for each of the materials is equal to the geometric mean of the values at the real and ghost node:

$$k_{\mathrm{rw}}^{I(jk)} = \sqrt{k_{\mathrm{rw}}^{I}\left(h_{\mathrm{w}}^{(j)}\right) \times k_{\mathrm{rw}}^{I}\left(h_{\mathrm{w}}^{(k)'}\right)} , \tag{4.79}$$

$$k_{\mathrm{rw}}^{II(jk)} = \sqrt{k_{\mathrm{rw}}^{II}\left(h_{\mathrm{w}}^{(j)'}\right) \times k_{\mathrm{rw}}^{II}\left(h_{\mathrm{w}}^{(k)}\right)} . \tag{4.80}$$

The nonlinear system of equations (4.77)–(4.78) has to be solved iteratively for each material interface. The inter-nodal conductivity is then computed as the harmonic average of the conductivities in two sub-layers:

$$K_{\mathrm{w}}^{(jk)} = \frac{2\, K_{\mathrm{sw}}^{I}\, k_{\mathrm{rw}}^{I(jk)}\, K_{\mathrm{sw}}^{II}\, k_{\mathrm{rw}}^{II(jk)}}{K_{\mathrm{sw}}^{I}\, k_{\mathrm{rw}}^{I(jk)} + K_{\mathrm{sw}}^{II}\, k_{\mathrm{rw}}^{II(jk)}} \tag{4.81}$$

While this method was shown to be more accurate than the standard arithmetic and geometric weighting of the nodal conductivities in the test cases considered by Romano et al. [32] and Brunone et al. [8], it raises two questions. First, it is not clear, why the pressure values at ghost nodes, which do not have any physical interpretation, should be used instead of the value of the pressure at the interface, as in Eq. (4.68). Second, geometric averaging of the relative permeabilities was shown to be very inaccurate in some problems involving homogeneous media, and one can expect similar type of errors in the heterogeneous case.

Szymkiewicz and Helmig [40] compared the performance of various permeability averaging schemes for one-dimensional incompressible flow in layered soils. Principal results of their investigation are presented here. Four approximation methods were used to compute the average permeability across a material interface separating sand and clay layers. They include Eqs. (4.68)–(4.72) combined with the method of Szymkiewicz [39] to evaluate the permeability at each side of the interface (referred to as CC-SZYM), the simple arithmetic averaging, Eq. (4.74)

Table 4.7 Parameters of soils used in the numerical simulations of steady-state flow in a heterogeneous medium. Modified with permission from [40]

Soil	θ_{rw} (–)	θ_{sw} (–)	p_e or p_g (Pa)	n_b or n_g (–)	K_{sw} ($m\,s^{-1}$)
BC-sand	0.020	0.417	711	0.592	5.83×10^{-5}
BC-clay	0.056	0.423	3360	0.127	2.50×10^{-7}
VGM-sand	0.043	0.430	677	2.68	8.25×10^{-5}
VGM-clay	0.007	0.360	19620	1.09	5.56×10^{-8}

(CC-ARIT), the combination of harmonic averaging of the intrinsic permeability and upstream weighting of the relative permeability, Eqs. (4.73), (4.75) and (4.76) (CC-UPS), and the method of Romano et al. [32] (CC-ROM). The results were compared to the values of the inter-nodal permeability obtained from the numerical solution of steady-state flow equation between the two points, using very fine spatial discretization. The two soils were characterized by either Brooks–Corey–Burdine or van Genuchten–Mualem functions. Their parameters are listed in Table 4.7. For each set of hydraulic functions, a large number of simulations was performed, with varying sequence of the layers (sand over clay, clay over sand), distance between nodes, $\Delta x = \{1, 2, 5, 10, 20, 50, 100, 200, 500\}$ cm, and potential head values at the nodes, $h_w = \{10, 0, -1, -10, -100, -1000\}$ cm (for Brooks–Corey model the potential values were modified by adding negative value corresponding to h_e, as listed in Table 4.7 for respective soils).

The error of each averaging scheme was defined similarly to Eq. (4.63). However, the values of total conductivity were used instead of the relative permeability:

$$\text{ERR-K} = \log_{10} \frac{K_w^{(jk)}}{K_{ref}^{(jk)}} \tag{4.82}$$

where $K_w^{(jk)}$ and $K_{ref}^{(jk)}$ denote, respectively, the approximate inter-nodal conductivity and the reference conductivity obtained from the steady-state solution. For each averaging method the root mean square, maximum and minimum error values were defined in the way described in Sect. 4.2.5. The values of these parameters are listed in Table 4.8 for soils characterized by Brooks-Corey functions and in Table 4.9 for the van Genuchten–Mualem functions. Additionally, for the schemes CC-ROM and CC-SZYM the values of the potential head at the interface $h_w^{(F)}$ can be compared with the values obtained from the numerical steady flow solution. The corresponding root mean square errors, denoted as RMS-ERR-H, are also reported.

The results shown in the tables indicate that the averaging scheme CC-SZYM, based on the approximation of the Darcian means, is much more accurate in predicting the value of steady-state average conductivity than the other three methods. CC-ROM is second best, but still can lead to over- or underestimation of the conductivity by several orders of magnitude. It can be also noted that all methods are less accurate for the van Genuchten–Mualem model than for the Brooks–Corey–Burdine model.

Table 4.8 Errors of permeability approximation schemes for steady-state flow in a heterogeneous medium, Brooks–Corey–Burdine functions. Reproduced with permission from [40]

Scheme	RMS-ERR-K (–)	max(ERR-K) (–)	min(ERR-K) (–)	RMS-ERR-H (m)
CC-ARIT	1.91	6.18	−0.24	–
CC-ROM	0.66	2.32	−2.77	0.1815
CC-UPS	1.56	5.46	−2.55	–
CC-SZYM	0.08	1.34	−0.32	0.0041

Table 4.9 Errors of permeability approximation schemes for steady-state flow in a heterogeneous medium, van Genuchten–Mualem functions. Reproduced with permission from [40]

Scheme	RMS-ERR-K (–)	max(ERR-K) (–)	min(ERR-K) (–)	RMS-ERR-H (m)
CC-ARIT	3.21	10.37	−0.28	–
CC-ROM	1.78	5.58	−7.30	23.42
CC-UPS	1.94	7.88	−3.71	–
CC-SZYM	0.10	0.07	−0.51	1.31

Moreover, Szymkiewicz and Helmig [40] carried out comparisons of various permeability averaging schemes for several unsteady flow problems, using both cell-centred and vertex-centred spatial discretizations. In cell-centred scheme they used the same four methods for approximating permeability at material interface, as in the steady state analysis described above. In the framework of vertex-centred approach, where the porous material between the nodes is always homogeneous, the inter-nodal permeabilities were computed as arithmetic averages, Eq. (4.4) (VC-ARIT), geometric average, Eq. (4.5) (VC-GEOM), upstream weighting, Eq. (4.12) (VC-UPS) and the method of Szymkiewicz [39] (VC-SZYM). Two examples from [40] are presented below.

The first example concerns vertical downward infiltration with prescribed water flux at the surface, see Fig. 4.10a for the details of the geometry and the initial and boundary conditions. The sand and clay layer are characterized by Brooks–Corey–Burdine hydraulic functions with the parameters listed in Table 4.7. Since the hydraulic conductivity of clay is much smaller than the conductivity of sand, after some time a saturated zone develops at the material interface. Figure 4.11 shows the distribution of the volumetric water content in the soil profile after 32 h of infiltration. The thick solid line denotes the reference solution obtained on a dense grid with $\Delta x = 1$ mm. One can note the presence of a fully saturated zone in the vicinity of the interface with the maximum values of $\theta_w = 0.417$ for sand and $\theta_w = 0.423$ for clay. Below the interface a relatively sharp wetting front can be observed in the clay layer, while above the interface the water content in sand also decreases rapidly. The simulations performed on a coarse grid with $\Delta x = 20$ cm show significant influence of the method used for computing inter-nodal

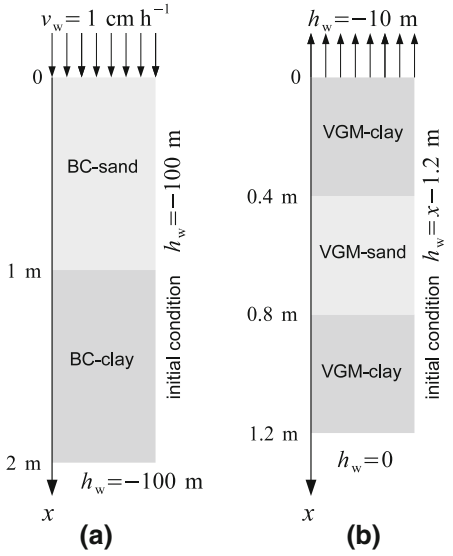

Fig. 4.10 Initial and boundary conditions used in simulations of flow in layered media. Modified with permission from [40]

permeabilities, for either vertex-centred (Fig. 4.11a) or cell-centred (Fig. 4.11b) discretization approaches. The results obtained with VC-SZYM and CC-SZYM schemes are relatively close to the reference solution. Similarly accurate results (not shown here) can be obtained with the method of Baker et al. [5]. In contrast, the schemes based on geometric averaging lead to very inaccurate profiles, with large saturated zone in the sand layer. The arithmetic and upstream weighting lead to moderately accurate solutions, which reproduce the general shape of the reference profile, but with more shifting and smoothing than the methods based on Darcian averaging.

In the second test case, evaporation from a three-layer soil profile was simulated. Evaporation was enforced by imposing a very large negative value of the pressure head at the soil surface. The details of the problem formulation are presented in Fig. 4.10b. The soil materials are characterized by van Genuchten–Mualem functions, with parameters listed in Table 4.7. A very long process was considered, with the final time equal to 5×10^4 h, and the cumulative amount of evaporated water equal to 7.26 cm, as predicted by the reference solution on fine grid ($\Delta x = 1$ mm). The coarse grid simulations with $\Delta x = 10$ cm predicted very different amounts of cumulative evaporation, depending on the applied method of permeability averaging. The relative error can be defined as:

$$\text{ERR-EV} = \frac{q_{\text{ev}} - q_{\text{ev}}^{\text{ref}}}{q_{\text{ev}}^{\text{ref}}} \times 100\,\% \tag{4.83}$$

where q_{ev} and $q_{\text{ev}}^{\text{ref}}$ denote the value of cumulative evaporation obtained in a given solution and the reference value, respectively. The relative errors are listed in

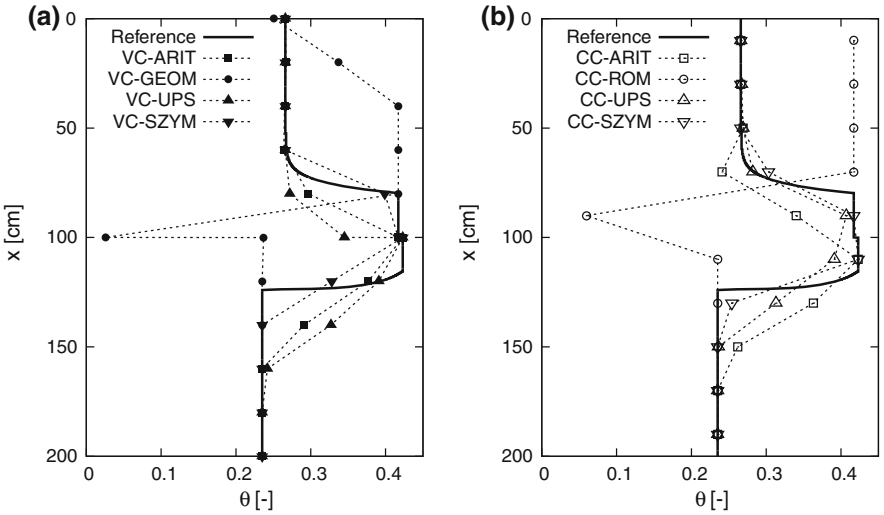

Fig. 4.11 Infiltration in layered medium: water content profiles obtained with vertex-centred (**a**) and cell-centred (**b**) schemes ($t = 32$ h, $\Delta x = 20$ cm). Reproduced with permission from [40]

Table 4.10. It can be seen that the smallest errors were obtained with the schemes based on the method of Szymkiewicz [39] and with the CC-UPS scheme. Arithmetic averaging and VC-UPS led to very large overestimation of the cumulative evaporation. In contrast, the schemes based on geometric mean significantly underestimated the evaporation. The profiles of the water pressure head at the end of simulation obtained using the same spatial discretization are shown in Fig. 4.12. They confirm high accuracy of the improved method of permeability averaging discussed in this work. The results obtained with VC-SZYM and CC-SZYM schemes are very close to the reference solution. In particular, these methods correctly predict the large gradient of the pressure head in the upper part of the central sand layer. Such a large gradient is necessary to sustain the upward flow in sand, as the relative permeability in the dry upper part of the sand layer is very small. Obviously, the accuracy in the the pressure gradient is strongly influenced by the accuracy in the inter-nodal permeability, as the product of these two values gives the volumetric water flux. The schemes VC-UPS, VC-ARIT and CC-ARIT overestimate the inter-nodal permeability. Therefore, the resulting gradients are smaller than in the reference solution. On the other hand, CC-ROM and VC-GEOM underestimate the inter-nodal permeability, leading to gradients much larger than in the reference profile.

For a finer discretization, $\Delta x = 1$ cm, the errors caused by arithmetic and upstream averaging significantly diminish, but they are still much larger than for the K-SZYM approach, with the exception of CC-UPS, which provides the most accurate results. The difference in performance between the two schemes based on upstream weighting, i.e. CC-UPS and VC-UPS, may be due to the fact that in VC

Table 4.10 Evaporation in a layered medium: relative errors in the cumulative amount of evaporated water for various permeability averaging schemes. Data from [40]

$\Delta x = 10$ cm				$\Delta x = 1$ cm			
Scheme	ERR-EV (%)	Scheme	ERR-EV (%)	Scheme	ERR-EV (%)	Scheme	ERR-EV (%)
CC-ARIT	400	VC-ARIT	237	CC-ARIT	19.7	VC-ARIT	16.4
CC-ROM	−59.1	VC-GEOM	−63.9	CC-ROM	−58.9	VC-GEOM	−59.3
CC-UPS	−9.63	VC-UPS	469	CC-UPS	2.11	VC-UPS	29.1
CC-SZYM	−2.33	VC-SZYM	−5.25	CC-SZYM	3.09	VC-SZYM	3.07

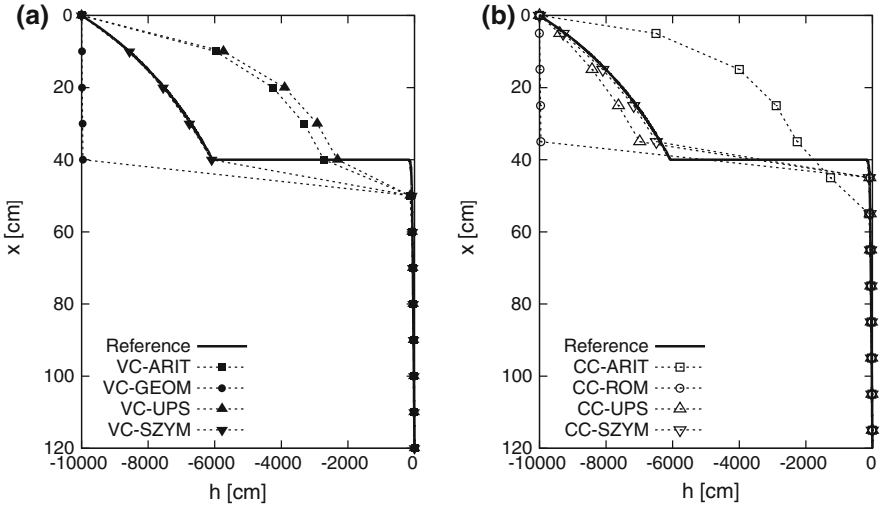

Fig. 4.12 Evaporation in a layered medium: pressure head profiles obtained with vertex-centred (**a**) and cell-centred (**b**) schemes ($t = 50000$ h, $\Delta x = 10$ cm). Reproduced with permission from [40]

scheme the change in water content at highly permeable side of the interface results in an immediate change in the part of the control volume located at the weakly permeable part of the interface. This is caused by the assumption of the continuity of the water pressure across the interface. If the control volumes at the interface are large, considerable amounts of water can move instantaneously across the interface. In the CC-UPS scheme, the interface coincides with the boundary between control volumes and harmonic averaging of the saturated conductivity (which gives more weight to the weakly permeable medium) partly compensates for the acceleration caused by upstream weighting of the relative conductivity [40]. Finally, it should be noted that in this numerical example the performance of the schemes based on geometric averaging (CC-ROM and VC-GEOM) does not improve as the grid is refined.

4.5 Multidimensional Problems

As shown in Chap. 3, permeability averaging in multidimensional problems can be carried out either using a finite-element like approach or a finite-difference like approach (used either in the finite difference or finite volume framework). In the first case, the permeability value at a specific point in the element is interpolated from the nodal values at all vertices of the element, or is evaluated as a function of the capillary pressure or water saturation at the considered point, which in turn is interpolated from the nodal pressures or saturations. In the second case, the permeability is evaluated at the midpoint of a primary grid edge, connecting two nodes. To this order many averaging schemes developed for one-dimensional flow can be used. However, their applicability depends on the properties of the numerical grid and the degree of anisotropy of the porous medium. Assuming that the spatial discretization is performed with the control volume finite element approach, several specific cases can be distinguished, as discussed below:

- *Isotropic permeability, rectangular grid*. In this case, all methods developed for one-dimensional flow can be used. The methods based on flux splitting and Darcian averaging can be expected to yield more accurate results, as they provide different relative permeabilities for horizontal and vertical fluxes.
- *Isotropic permeability, unstructured grid*. All simple averaging methods can be used, as well as the flux splitting methods, if one takes into account that the value of the gravitational coefficient ζ varies from one edge to the other, depending on their orientation with respect to the gravity vector. In the group of Darcian means, the variability of gravitational coefficient is included in the method of Szymkiewicz [39], and can be easily introduced in the methods of Baker [2] and Baker et al. [5], as shown in Sect. 4.1.3.
- *Diagonally anisotropic permeability, rectangular grid*. If the main anisotropy axes are aligned with the axes of spatial coordinate system and with the grid lines, the permeability in each direction can be computed with the one-dimensional approach. The relative permeability functions can be different in the horizontal and vertical direction.
- *Anisotropic intrinsic permeability, isotropic relative permeability, arbitrary grid*. For anisotropic media, the flux along specific edge depends on the components of the water potential gradient in both parallel and perpendicular directions. It means that the one-dimensional steady-state analysis, which is the basis of the Darcian averaging schemes, does not hold strictly. However, such methods can still be used to approximate the scalar relative permeability, which is then multiplied by the intrinsic permeability tensor.
- *Anisotropic intrinsic and relative permeability, arbitrary grid*. In this case, it is impossible to define the relative permeability function for an arbitrary direction. Therefore, methods based on the integration of the relative permeability function, including the integrated mean and Darcian mean approaches, cannot be used. In contrast, methods based on averaging of the nodal permeability values can be still applied, for example by averaging each component of the permeability tensor

separately. Upstreaming can be easily implemented assuming that the permeability tensor is positively definite, which in the context of groundwater flow means that the flux is directed from the node with larger potential to the node with lower potential.

In all the above cases, the permeability averaging is performed within a materially homogeneous grid element, according to the vertex-centred discretization scheme. In a heterogeneous medium, the inter-nodal permeabilities are calculated separately for the elements at each side of the edge, using the same pair of nodal pressures and different relative permeability functions. In some cases, the methods based on Darcian mean concept can be applied for multidimensional problems also in the framework of the cell-centred discretization, which implies the existence of material interfaces between nodes. This is possible if the medium is diagonally anisotropic and the grid is rectangular. In such a case, the interface condition given by Eq. (4.68) can be easily formulated for each spatial direction and the relative permeabilities at each side of the interface can be computed using more accurate formulae. However, in a more general case of unstructured cell-centred grids, one-dimensional Darcian approximations cannot be easily implemented.

In order to show the applicability of the improved averaging scheme [39] to two-dimensional flow in an isotropic medium, a comparison of the numerical results with the analytical solution of Tracy [42] is performed. The flow domain is a square $L_1 = 1\,\mathrm{m}$ by $L_2 = 1\,\mathrm{m}$, with x_1 axis horizontal and x_2 axis oriented vertically upward. The capillary and relative permeability functions are formulated with respect to the water pressure head h_w and have the exponential form:

$$\theta_\mathrm{w} = \theta_\mathrm{rw} + (\theta_\mathrm{sw} - \theta_\mathrm{rw}) \exp(h_\mathrm{w}/h_\mathrm{g}) \,, \tag{4.84}$$

$$K_\mathrm{w} = K_\mathrm{sw} \exp(h_\mathrm{w}/h_\mathrm{g}) \,, \tag{4.85}$$

with the parameters $\theta_\mathrm{sw} = 0.45$, $\theta_\mathrm{rw} = 0.15$, $h_\mathrm{g} = 2\,\mathrm{m}$ and $K_\mathrm{sw} = 10^{-5}\,\mathrm{m\,s^{-1}}$. The compressibility of soil and water is neglected. As the initial condition, a uniform distribution of the water pressure $h_\mathrm{w}^\mathrm{init} = -10\,\mathrm{m}$ is assumed. Along the bottom and the vertical sides of the domain this value is maintained as the boundary condition. At the top boundary a sinusoidal distribution of the pressure head is imposed:

$$h_\mathrm{w}^\mathrm{top}(x_1) = h_\mathrm{g} \ln\left[\exp\left(\frac{h_\mathrm{w}^\mathrm{init}}{h_\mathrm{g}}\right) + \left(1 - \exp\left(\frac{h_\mathrm{w}^\mathrm{init}}{h_\mathrm{g}}\right)\right) \sin\left(\frac{\pi x_1}{L_1}\right)\right] \tag{4.86}$$

For the above assumptions the value of the water pressure for a given spatial point (x_1, x_2) and time t can be calculated analytically as [42]:

$$h_{\mathrm{w}}(x_1, x_2, t) = h_{\mathrm{g}} \ln \left\{ \exp\left(\frac{h_{\mathrm{w}}^{\mathrm{init}}}{h_{\mathrm{g}}}\right) + h'' \sin\frac{\pi x_1}{L_1} \exp\left(\frac{L_2 - x_2}{2\, h_{\mathrm{g}}}\right) \left[\frac{\sinh(\beta'' x_2)}{\sinh(\beta'' L_2)} + \frac{2}{L_2\, c''} \sum_{n=1}^{\infty} (-1)^n \frac{\lambda_n''}{\gamma''} \sin(\lambda_n'' x_2) \exp(-\gamma'' t) \right] \right\} \tag{4.87}$$

where:

$$c'' = \frac{(\theta_{\mathrm{sw}} - \theta_{\mathrm{rw}})}{h_{\mathrm{g}}\, K_{\mathrm{sw}}}, \quad \gamma'' = \frac{(\beta'')^2 + (\lambda_n'')^2}{c''}, \quad \lambda_n'' = \frac{n\,\pi}{L_2},$$

$$\beta'' = \sqrt{\frac{1}{4\,(h_{\mathrm{g}})^2} + \left(\frac{\pi}{L_1}\right)^2}, \quad h'' = 1 - \exp(h_{\mathrm{w}}^{\mathrm{init}}/h_{\mathrm{g}}).$$

Numerical simulations were performed using both rectangular and unstructured (triangular) meshes. For each mesh type, two levels of refinement were considered: a coarser one with $\Delta x = 10\,\mathrm{cm}$ and a finer one with $\Delta x = 2\,\mathrm{cm}$. In the case of unstructured grid, these values refer to the node spacing imposed along the boundaries of the domain. The unstructured mesh was generated using NetGen code, developed by Burzyński [9]. The vertex centred finite volume approach was used with two-point approximation of the average permeability at each cell face, which allowed for the use of various schemes developed for one-dimensional flow. The pressure gradient was evaluated using the finite element approach. For structured meshes the evaluation point was chosen as either the edge midpoint or the face midpoint, as shown in Chap. 3, Fig. 3.4. In the first case the scheme becomes equivalent to the finite difference scheme, and is denoted by FD. For each simulation the root mean square error of the nodal values of the water pressure at the final time $t = 720\,\mathrm{s}$ was computed:

$$RMSE_p = \sqrt{\frac{1}{N} \sum_{1}^{N} (p_{\mathrm{num}} - p_{\mathrm{ref}})^2} \tag{4.88}$$

where N is the number of internal nodes in the domain, p_{num} is the final water pressure at a specific node from the numerical solution and p_{ref} is the corresponding pressure value obtained from the analytical solution ($p_{\mathrm{w}} = h_{\mathrm{w}}\, \rho_{\mathrm{w}}\, g$). The values of RMSE for different grids and permeability averaging schemes are listed in Table 4.11.

It can be seen that the permeability averaging schemes K-SZYM and K-BAKER are significantly more accurate than the other approaches. In this test case, the flow is dominated by capillary forces and K-SZYM is equivalent to the integrated mean method. On the other hand, for exponential permeability function K-BAKER represents the exact solution of steady-state flow. Thus, one could expect K-BAKER to be the most accurate of all methods. However, the results show that it is slightly less accurate than K-SZYM. This apparent contradiction can be explained by the fact that

Table 4.11 Example 7: root mean square errors in the water pressure (Pa) for different numerical approximation schemes

Grid	K-SZYM	K-BAKER	K-GEOM	K-ARIT	K-UPS
Structured, FD					
Fine	32	35	271	388	1915
Coarse	836	911	1036	2183	6308
Structured, FE					
Fine	29	31	271	389	1914
Coarse	676	746	920	2160	6298
Unstructured, FE					
Fine	39	39	219	322	1634
Coarse	502	536	979	1754	5334

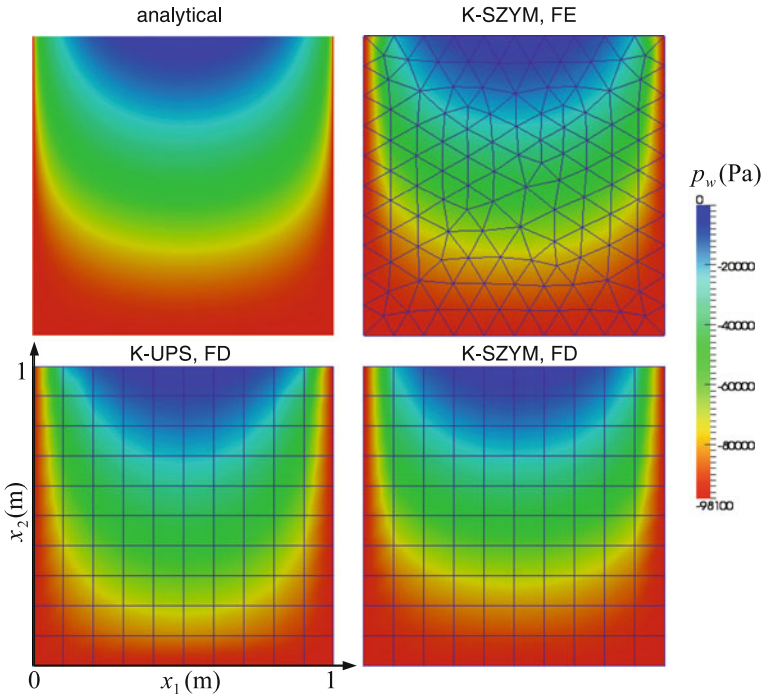

Fig. 4.13 Example 7: water pressure distribution for the final time $t = 720$ s according to the analytical solution and three numerical solutions of coarse grid

applying steady-state results to transient flow introduces additional error. It should be also noted that for this particular setting the geometric mean is more accurate than the arithmetic mean, while the upstream weighting produces considerable errors, even on finer grids.

In Fig. 4.13 the distribution of the water pressure for $t = 720$ s obtained with the K-SZYM method on structured and unstructured coarse grids is compared to

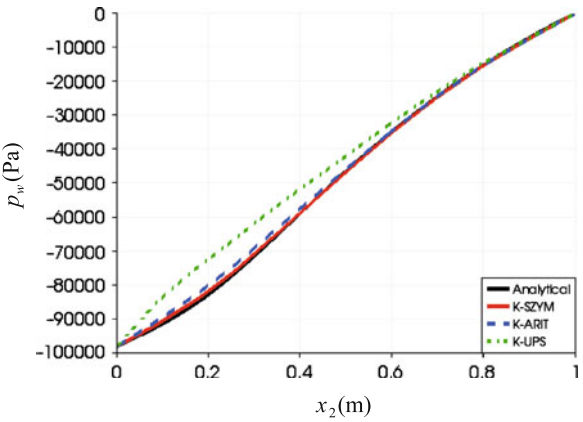

Fig. 4.14 Example 7: water pressure profile along the vertical symmetry axis according to the analytical solution and three numerical solutions of coarse grid ($t = 720$ s)

the analytical solution and to the solution on structured grid using K-UPS averaging scheme. The plots are consistent with the error measures reported in Table 4.11. The solutions obtained using K-SZYM scheme are in a very good visual agreement with the reference analytical solution, while K-UPS predicts a more diffuse wetting front. Figure 4.14 shows the water pressure profiles along the vertical symmetry axis at the end of the simulation obtained for the coarse unstructured grid using K-SZYM, K-ARIT and K-UPS. It can be seen that the result for K-SZYM is virtually the same as the analytical solution, K-ARIT gives a slight discrepancy, while K-UPS predicts significantly different profile shape.

4.6 Two-Phase Flow

The development of approximate Darcian averages, such as the ones presented in Sect. 4.2, is not possible for two-phase flow, because the relative permeability depends on the pressures in both fluid phases. In contrast, the simple averaging methods such as the arithmetic, geometric, harmonic and upstream mean can be in principle used to compute the inter-nodal permeability for each of the fluid phases. It is also possible to define an integrated mean for each fluid phase by integrating the relative permeability with respect to the capillary pressure:

$$k_{\mathrm{rw}}^{(ij)} = \frac{1}{p_{\mathrm{c}}^{(j)} - p_{c}^{(i)}} \int_{p_{\mathrm{c}}^{(i)}}^{p_{\mathrm{c}}^{(j)}} k_{\mathrm{rw}}(\hat{p})\, \mathrm{d}\hat{p} \tag{4.89}$$

$$k_{\mathrm{ra}}^{(ij)} = \frac{1}{p_{\mathrm{c}}^{(j)} - p_{\mathrm{c}}^{(i)}} \int_{p_{\mathrm{c}}^{(i)}}^{p_{\mathrm{c}}^{(j)}} k_{\mathrm{ra}}(\hat{p})\, \mathrm{d}\hat{p} \tag{4.90}$$

It should be noted that the above formula for k_{rw} is equivalent to the integrated mean developed for the Richards equation, Eq. (4.9), only if the air pressure is atmospheric ($p_{\mathrm{a}} = 0$) and both nodes are unsaturated.

The two-phase flow model includes advective terms related to viscous and gravity forces, as well as the capillary diffusion term. The Richards equation represents a limit case where the viscous forces are negligible and only capillary and gravity terms remain. Thus some insights into the problem of permeability averaging for two phase flow can be gained from the analysis of the Richards equation presented in the above sections. In particular, one can expect that if the pressure gradients in the air phase are negligible, the average permeability of the water phase will vary in the range from the integrated mean (for capillary dominated flow) to the permeability of the upper node (for gravity dominated flow), with the arithmetic mean being a reasonable approximation for intermediate conditions. This is confirmed by numerical solutions of Celia and Binning [10] and Kees and Miller [24], who employed arithmetic averaging, and Touma and Vauclin [41], who used geometric averaging on a relatively fine grid. On the other hand, if significant pressure gradients exist in the non-wetting phase, the role of advective terms related to the viscous forces increases. Consequently, arithmetic, geometric or integrated averaging will produce oscillatory solutions, which can be avoided by employing upstream average. Permeability upstreaming is commonly used for two-phase flow with non-wetting to wetting phase mobility ratio close to one or smaller than one, e.g. in liquid hydrocarbons—water system [22]. However, the application of upstreaming for capillary driven two-phase flow in air-water system may lead to overly diffusive and inaccurate solutions. An approach alternative to upstreaming is the explicit addition of artificial diffusion to the discrete equations. This method was applied in [20] for the fractional flow formulation.

The influence of the permeability averaging method on the solution of one-dimensional two phase flow equations was investigated in the framework of the finite element discretization by Helmig and Huber [22], and in the framework of the finite volume formulation by Szymkiewicz [38]. In the following two other illustrative examples are presented. In the first test case, one-dimensional, horizontal, capillary dominated flow is considered. The dimension of the solution domain is 0.5 m and the soil is characterized by Brooks–Corey–Burdine hydraulic functions with the following parameters: $\phi = 0.4$, $S_{\mathrm{rw}} = S_{\mathrm{ra}} = 0$, $k = 1.25 \times 10^{-12}\,\mathrm{m}^2$, $p_{\mathrm{e}} = 814\,\mathrm{Pa}$, $n_{\mathrm{b}} = 0.686$. The compressibility of water and soil is neglected. Initially, the pore air is at atmospheric pressure ($p_{\mathrm{a}} = 0$) and the water saturation is $S_{\mathrm{w}} = 0.1$. At the left-hand side boundary ($x = 0$), a constant value of water saturation $S_{\mathrm{w}} = 0.95$ is

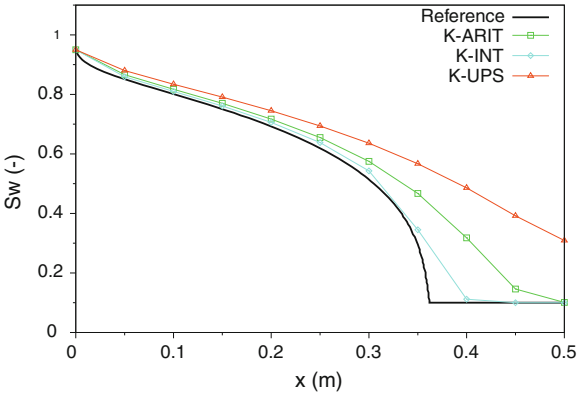

Fig. 4.15 Water saturation profiles for two-phase horizontal flow ($t = 4$ h)

imposed, while the air phase is maintained at atmospheric pressure. The right-hand side boundary is assumed to be impermeable for both fluids ($v_w = v_a = 0$). For such conditions, a semi-analytical solution of Sunada and McWhorter [37] can be applied. The semi-analytical solution is computed following the improved method by Fucik et al. [18]. It is compared to the results of the numerical simulations using three permeability averaging schemes: the upstream weighting, arithmetic averaging and integrated averaging with respect to the $k_\alpha(p_c)$ function. For a fine grid, $\Delta x = 0.5$ cm, all three approaches gave results very close to the analytical solution (results not shown here). For a coarser grid with $\Delta x = 5$ cm, significant differences occur, as shown in Fig. 4.15. The integrated mean provides results very close to the reference solution, while K-ARIT and K-UPS lead to more diffuse wetting fronts, which in the case of K-UPS reaches the boundary of the domain. Note that the same relative accuracy of the three methods is observed for the Richards equation if the flow is capillary-dominated, which is the case for horizontal flow or vertical flow with small Δx, as shown in Example 1, Fig. 4.6.

In the final example, vertical two phase flow is considered. The geometry, soil parameters and initial conditions are the same as in the previous case. The boundary conditions correspond to ponded infiltration, i.e. at the top of the soil layer $p_w = 100$ Pa and $S_w = 1$, while at the bottom the initial values of the water pressure and saturation are maintained. In this case no analytical solution can be applied and a numerical solution on dense grid $\Delta x = 0.05$ cm is considered as the reference. The coarse grid solutions ($\Delta x = 0.5$ cm) shown in Fig. 4.16 behave differently from the previous case. The integrated mean underestimates the position of the wetting front, while the upstream weighting and arithmetic averaging are more accurate with respect to the position of the front, but show more significant numerical diffusion, especially in the case of upstream weighting.

An additional issue arises when a part of the solution domain is fully saturated with water and the medium has a non-zero value of the entry pressure. In such a case, the air pressure at the water-saturated nodes is physically undefined, but in the

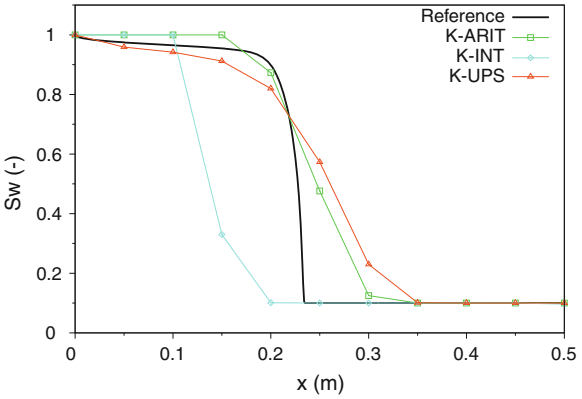

Fig. 4.16 Water saturation profiles for two-phase vertical flow ($t = 3$ h)

numerical algorithm it is computed as $p_a = p_w + p_e$, and thus can be higher than the atmospheric pressure. If air at atmospheric pressure is present at a neighboring node, a gradient in the air potential occurs between the water-saturated node and the unsaturated node, even though physically no flow is possible. The average air permeability in this case should be equal to zero, which is naturally accounted for by the use of upstream weighting and geometric averaging. For other averaging formulae, appropriate modifications have to be made to prevent non-physical fluxes.

The above examples show that there is a potential for improvement of the permeability averaging formulas for the two-phase flow, based on the relations between capillary, gravity and viscous forces at the scale of a single numerical grid cell. However, such an analysis is beyond the scope of the present work.

References

1. Aziz K, Settari A (1979) Petroleum reservoir simulation. Applied Science, Essex
2. Baker D (1995) Darcian weighted interblock conductivity means for vertical unsaturated flow. Ground Water 33(3):385–390. doi:10.1111/j.1745-6584.1995.tb00294.x
3. Baker D (2000) A Darcian integral approximation to interblock hydraulic conductivity means in vertical infiltration. Comput Geosci 26(5):581–590
4. Baker D (2006) General validity of conductivity means in unsaturated flow. J Hydrol Eng 11(6):526–538
5. Baker D, Arnold M, Scott H (1999) Some analytic and approximate Darcian means. Ground Water 37(4):532–538. doi:10.1111/j.1745-6584.1999.tb01139.x
6. Belfort B, Lehmann F (2005) Comparison of equivalent conductivities for numerical simulation of one-dimensional unsaturated flow. Vadose Zone J 4(4):1191–1200
7. Berg P (1999) Long-term simulation of water movement in soils using mass-conserving procedures. Adv Water Resour 22(5):419–430
8. Brunone B, Ferrante M, Romano N, Santini A (2003) Numerical simulations of one-dimensional infiltration into layered soils with the Richards' equation using different enstimates of the interlayer conductivity. Vadose Zone J 2(2):193–200

9. Burzyński K, Szymkiewicz A (2011) Unstructured finite-volume meshes for two-dimensional flow in variably saturated porous media. TASK Q 15(3):1001–10,014
10. Celia M, Binning P (1992) A mass conservative numerical solution for two-phase flow in porous media with application to unsaturated flow. Water Resour Res 28(10):2819–2828
11. Celia M, Bouloutas E, Zarba R (1990) A general mass-conservative numerical solution for the unsaturated flow equation. Water Resour Res 26(7):1483–1496
12. Desbarats A (1995) An interblock conductivity scheme for finite difference models of steady unsaturated flow in heterogeneous media. Water Resour Res 31(11):2883–2889
13. Fagerlund F, Niemi A, Odén M (2006) Comparison of relative permeabilityfluid saturationcapillary pressure relations in the modelling of non-aqueous phase liquid infiltration in variably saturated, layered media. Adv Water Resour 29(11):1705–1730. doi:10.1016/j.advwatres.2005.12.007
14. Fletcher C (1991) Computational techniques for fluid dynamics 1. Fundamental and general techniques. Springer, Berlin
15. Forsyth P, Kropinski M (1997) Monotonicity considerations for saturated–unsaturated subsurface flow. SIAM J Sci Comput 18(5):1328–1354
16. Forsyth P, Wu Y, Pruess K (1995) Robust numerical methods for saturated–unsaturated flow in heterogeneous media. Adv Water Resour 18(1):25–38
17. Fuhrmann J, Langmach H (2001) Stability and existence of solutions of time-implicit finite volume schemes for viscous nonlinear conservation laws. Appl Numer Math 37(1–2):201–230
18. Fučik R, Mikyška J, Beneš M, Illangasekare T (2007) An improved semi-analytical solution for verification of numerical models of two-phase flow in porous media. Vadose Zone J 6(1):93–104
19. Gastó J, Grifoll J, Cohen Y (2002) Estimation of internodal permeabilities for numerical simulations of unsaturated flows. Water Resour Res 38(12):1326
20. Guarnaccia J, Pinder G, Fishman M (1997) NAPL: simulator documentation. Environmental Protection Agency, USA
21. Haverkamp R, Vauclin M (1979) A note on estimating finite difference interblock hydraulic conductivity values for transient unsaturated flow. Water Resour Res 15(1):181–187
22. Helmig R, Huber R (1998) Comparison of Galerkin-type discretization techniques for two-phase flow in heterogenous porous media. Adv Water Resour 21(8):697–711
23. Kavetski D, Binning P, Sloan S (2001) Adaptive time stepping and error control in a mass conservative numerical solution of the mixed form of Richards equation. Adv Water Resour 24(6):595–605
24. Kees C, Miller C (2002) Higher order time integration methods for two-phase flow. Adv Water Resour 25(2):159–177
25. Kirkland M, Hills R, Wierenga P (1992) Algorithms for solving Richards equation for variably saturated soil. Water Resour Res 28(8):2049–2058
26. Kueper B, Frind E (1991) Two-phase flow in heterogeneous porous media 1. Model development. Water Resour Res 27(6):1049–1057
27. Lassabatere L, Angulo-Jaramillo R, Cuenca R, Braud I, Haverkamp R (2006) Beerkan estimation of soil transfer parameters through infiltration experiments—BEST. Soil Sci Soc Am J 70(2):521–532
28. Lima-Vivancos V, Voller V (2004) Two numerical methods for modeling variably saturated flow in layered media. Vadose Zone J 3(3):1031–1037
29. Manzini G, Ferraris S (2004) Mass-conservative finite volume methods on 2-d unstructured grids for the Richards' equation. Adv Water Resour 27(12):1199–1215
30. Miller C, Williams G, Kelley C, Tocci M (1998) Robust solution of Richards equation for nonuniform porous media. Water Resour Res 34(10):2599–2610
31. Pei Y, Wang J, Tian Z, Yu J (2006) Analysis of interfacial error in saturated–unsaturated flow models. Adv Water Resour 29(4):515–524
32. Romano N, Brunone B, Santini A (1998) Numerical analysis of one-dimensional unsaturated flow in layered soils. Adv Water Resour 21(4):315–324

33. Ross P (2003) Modeling soil water and solute transport—fast simplified numerical solutions. Agron J 95(6):1352–1361
34. Schnabel R, Richie E (1984) Calculation of internodal conductances for unsaturated flow simulations. Soil Sci Soc Am J 48(5):1006–1010
35. Šimnek J, Šejna M, Saito H, Sakai M, van Genuchten M (2008) The HYDRUS-1D software package for simulating the one-dimensional movement of water, heat and multiple solutes in variably-saturated media. Version 4.0. Department of Environmental Sciences, University of California Riverside, Riverside
36. Srivastava R, Guzman-Guzman A (1995) Analysis of hydraulic conductivity averaging schemes for one-dimensional, steady-state unsaturated flow. Ground Water 33(6):946–952. doi:10.1111/j.1745-6584
37. Sunada D, McWhorter D (1990) Exact integral solutions for two phase flow. Water Resour Res 26(3):399–413
38. Szymkiewicz A (2007) Numerical simulation of one-dimensional two-phase flow in porous media. Arch Hydro-eng Environ Mech 54(2):117–136
39. Szymkiewicz A (2009) Approximation of internodal conductivities in numerical simulation of 1D infiltration, drainage and capillary rise in unsaturated soils. Water Resour Res 45:W10403
40. Szymkiewicz A, Helmig R (2011) Comparison of conductivity averaging methods for one-dimensional unsaturated flow in layered soils. Adv Water Resour 34(8):1012–1025
41. Touma J, Vauclin M (1986) Experimental and numerical analysis of two-phase infiltration in a partially saturated soil. Transp Porous Media 1(1):27–55
42. Tracy F (2006) Clean two and three-dimensional analytical solutions of Richards' equation for testing numerical solvers. Water Resour Res 42:W08503
43. van Dam J, Feddes R (2000) Numerical simulation of infiltration, evaporation and shallow groundwater levels with the Richards equation. J Hydrol 233(1):72–85
44. Warrick A (1991) Numerical approximation of Darcian flow through unsaturated soil. Water Resour Res 27(6):1215–1222
45. Warrick A, Yeh TC (1990) One-dimensional, steady vertical flow in a layered soil profile. Adv Water Resour 13(4):207–210
46. Zaidel J, Russo D (1992) Estimation of finite difference interblock conductivities for simulation of infiltration into initially dry soils. Water Resour Res 28(9):2285–2295
47. Zhang X, Ewen J (2000) Efficient method for simulating gravity-dominated water flow in unsaturated soils. Water Resour Res 36(9):2777–2780